Science of the Total Environment 739 (2020) 139959

Contents lists available at ScienceDirect

Science of the Total Environment

journal homepage: www.elsevier.com/locate/scitotenv

Hydrogeological constraints for the genesis of the extreme lithium enrichment in the Salar de Atacama (NE Chile): A thermohaline flow modelling approach

M.A. Marazuela [a,b,*], C. Ayora [a], E. Vázquez-Suñé [a], S. Olivella [b], A. García-Gil [c]

[a] Institute of Environmental Assessment and Water Research (IDAEA), CSIC, Jordi Girona 18-26, 08034 Barcelona, Spain
[b] Department of Civil and Environmental Engineering, Technical University of Catalonia (UPC), Jordi Girona 1-3, 08034 Barcelona, Spain
[c] Geological and Mining Institute of Spain (IGME), Manuel Lasala 44, 9° B, 50006 Zaragoza, Spain

HIGHLIGHTS

- The thermohaline groundwater flow of the Salar de Atacama basin is modelled.
- The most evaporated brines converge towards the eastern edge of the Salar de Atacama.
- A saline interface isolates the nucleus from external groundwater flow contributions.
- Li enrichment can be explained by remobilization of buried Li-rich salt/clays.
- Convection in faults can favour the extreme Li enrichment of dilute inflows.

GRAPHICAL ABSTRACT

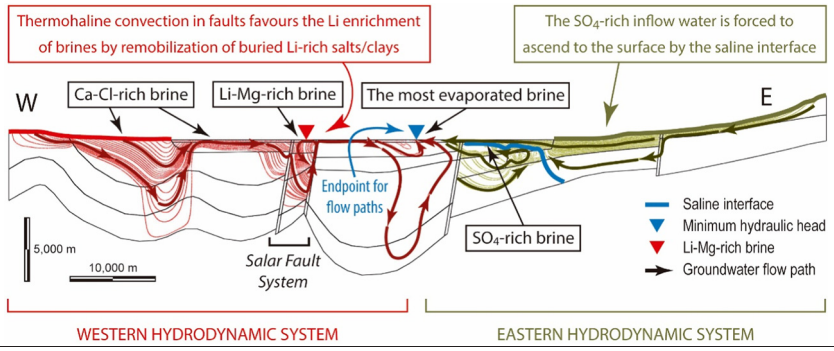

ARTICLE INFO

Article history:
Received 15 March 2020
Received in revised form 23 May 2020
Accepted 2 June 2020
Available online 7 June 2020

Editor: Jurgen Mahlknecht

Keywords:
Saline interface
Density-driven flow
Convection
Brine
Groundwater flow
Fault

ABSTRACT

The Salar de Atacama (SdA) is the largest Li reserve globally. The origin of Li, together with the rest of solutes, has been object of debate. Thus, rock weathering at low temperature, hydrothermal leaching or magmatic origin together with subsequent evaporation has been hypothesized. However, the extreme Li enrichment (>4000 mg/L) and the location of the Li-Mg-rich brines around the Salar Fault System (SFS) that crosses the nucleus of the SdA in half remain unexplained. The objective of this work is to define the thermohaline groundwater flow in the SdA basin to account for the genesis of its extreme Li enrichment.

Thermohaline flow modelling has demonstrated the critical effect of the minimum hydraulic head (MHH) of the regional water table on the groundwater flow of salt flats. The MHH divides the basin into two isolated hydrodynamic systems and constitutes the endpoint towards which the most evaporated brines converge. The spatial mismatch between the locations of the Li-Mg-rich brines in the central-western zone of the nucleus (in the SFS) and the MHH in the easternmost zone of the nucleus discards recent evaporative concentration of the recharge water as the main mechanism of Li enrichment. Moreover, the persistence of a saline interface surrounding the nucleus at depth, regardless of the temperature gradient, also precludes lateral recharge (predominantly from the east) to ascend along the SFS.

On the other hand, the computed thermohaline flow is compatible with the remobilization of buried layers of Li-Mg-enriched salts and/or clays by dilute recharge waters coming from the west or southwest of the basin. Here, the role of faults and density-driven flow is key to allow efficient downward and upward flow rates that favour the remobilization of Li and Mg.

* Corresponding author at: Institute of Environmental Assessment and Water Research (IDAEA), CSIC, Jordi Girona 18-26, 08034 Barcelona, Spain.
E-mail address: mamarazuela@outlook.com (M.A. Marazuela).

https://doi.org/10.1016/j.scitotenv.2020.139959
0048-9697/

1. Introduction

The intense evaporation (mainly phreatic evaporation) that occurs in salt flats (*salars*) contributes to the enrichment in Li, B, I, K, Mg and NaCl, which are very attractive for mining exploitation (Baspineiro et al., 2020; Eugster, 1980; Hardie et al., 1978; Liu et al., 2019; Liu and Agusdinata, 2020; Rosen, 1994; Wood and Sanford, 1990; Yechieli and Wood, 2002; Zatout et al., 2020). The brines of salt flats account for 80% of the world's reserves of Li. This element is essential for the development of mobile phone and electric vehicle batteries, as well as in the pharmacology industry (USGS, 2019). The largest salt flats on earth are located in the Central Andes, which includes northwestern Argentina, southwestern Bolivia and northeastern Chile (Warren, 2016, 2010). Approximately 25% of the global Li reserves are in the Salar de Atacama (SdA) (northeast Chile), which is located in the Pre-Andean Depression to the west of the Altiplano-Puna (Fig. 1). The SdA is formed by a halite nucleus filled by interstitial brine in the centre of the basin and a marginal zone composed of gypsum and carbonates around it, which features outcrops of the mixing zone (saline interface) resulting from the density contrast between the freshwater (1000 kg/m^3) coming from the recharge in the mountains and the brine (1200 kg/m^3) of the nucleus (Marazuela et al., 2018, 2019a). The nucleus is divided into two blocks by the north-northwestern-trending Salar Fault System (SFS) located in its central-western zone (Figs. 1 and 2). The pores and cavities of the nucleus are filled with SO_4-rich brines in the eastern block, Ca-Cl-rich brines in the western block and Li-Mg-rich brines (>4000 mg/L) in the area around the SFS closest to the Cordón de Lila (Ide and Kunasz, 1990; Kesler et al., 2012; Munk et al., 2018; Risacher and Alonso, 1996) (Fig. 2).

The origin of solutes in salt flats has been extensively studied in recent decades, mainly using solute chemistry and isotopic data. Both volcanic fluids and weathering of volcanic rocks have been proposed as primary sources for Li and other solutes in the Andean salt flats (Alonso and Risacher, 1996; Alpers and Whittemore, 1990; Risacher et al., 2003; Risacher and Alonso, 1996; Risacher and Fritz, 2009, 1991, among others). Regardless their origin, the dilute concentration of Li in the surface and groundwater recharge and in the geothermal fluids of the region (commonly below 50 mg/L, Godfrey et al., 2019) make necessary to consider an additional concentration process to explain the extremely high Li concentrations in the SFS.

Munk et al. (2016) described the formation of Li-rich brines worldwide as a result of groundwater flow paths converging into endorheic basins and discharge through evaporation, concentrating the solutes and resulting in precipitated salts and highly concentrated brines. Referring to Andean salt flats in general, Risacher et al. (2003) proposed evaporation and recycling of brines (leached of buried salt flats or leaked from present-day salt flats) as the mechanisms to explain the chemistry of some salt flats. Thus, depending on the inflow water, the evaporative concentration would lead to Ca-Cl-rich and SO_4-rich brine. The infiltrating brines would mix with diluted meteoric water forming recycling cells. The heat flow would act as a driving force for these recycling cells, possibly resulting in very complex mixing patterns. For the SdA in particular, Risacher and Fritz (2009) described a system in which each brine is related to the lithology of its drainage basin (Fig. 3A). Thus, sedimentary-evaporitic rocks in the western flank of the basin result in Ca-Cl-rich brines, and volcanic rocks in the eastern flank of the basin lead to SO_4-rich brines. These authors concluded that no inflow currently enters the nucleus from the west and, therefore, the Ca-Cl-rich brine formed in ancient times and could be entirely replaced by the SO_4-rich brines inflowing from the east in the future.

More recently, based on an important deficit in salt mass balance, Corenthal et al. (2016) proposed that the SdA topographic watershed does not coincide with the hydrogeological watershed (Fig. 3B). Using multi-element, multi-isotope and statistical approaches, Rissmann

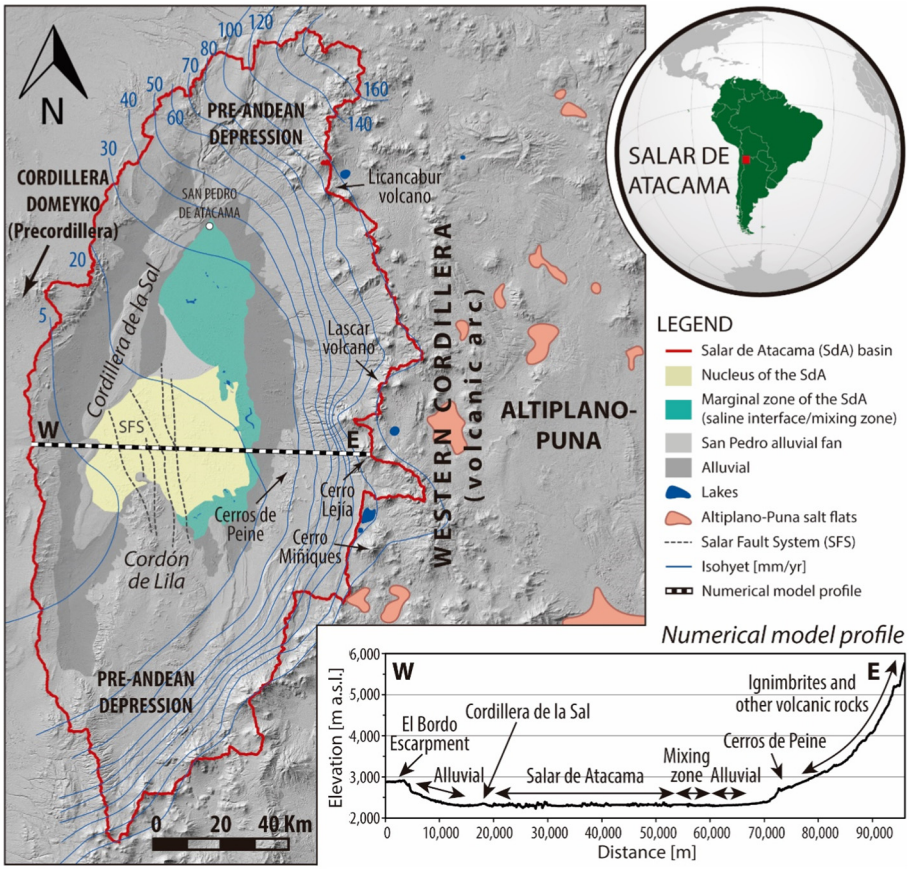

Fig. 1. Location of the Salar de Atacama basin. Also the topography of the numerical model profile is shown.

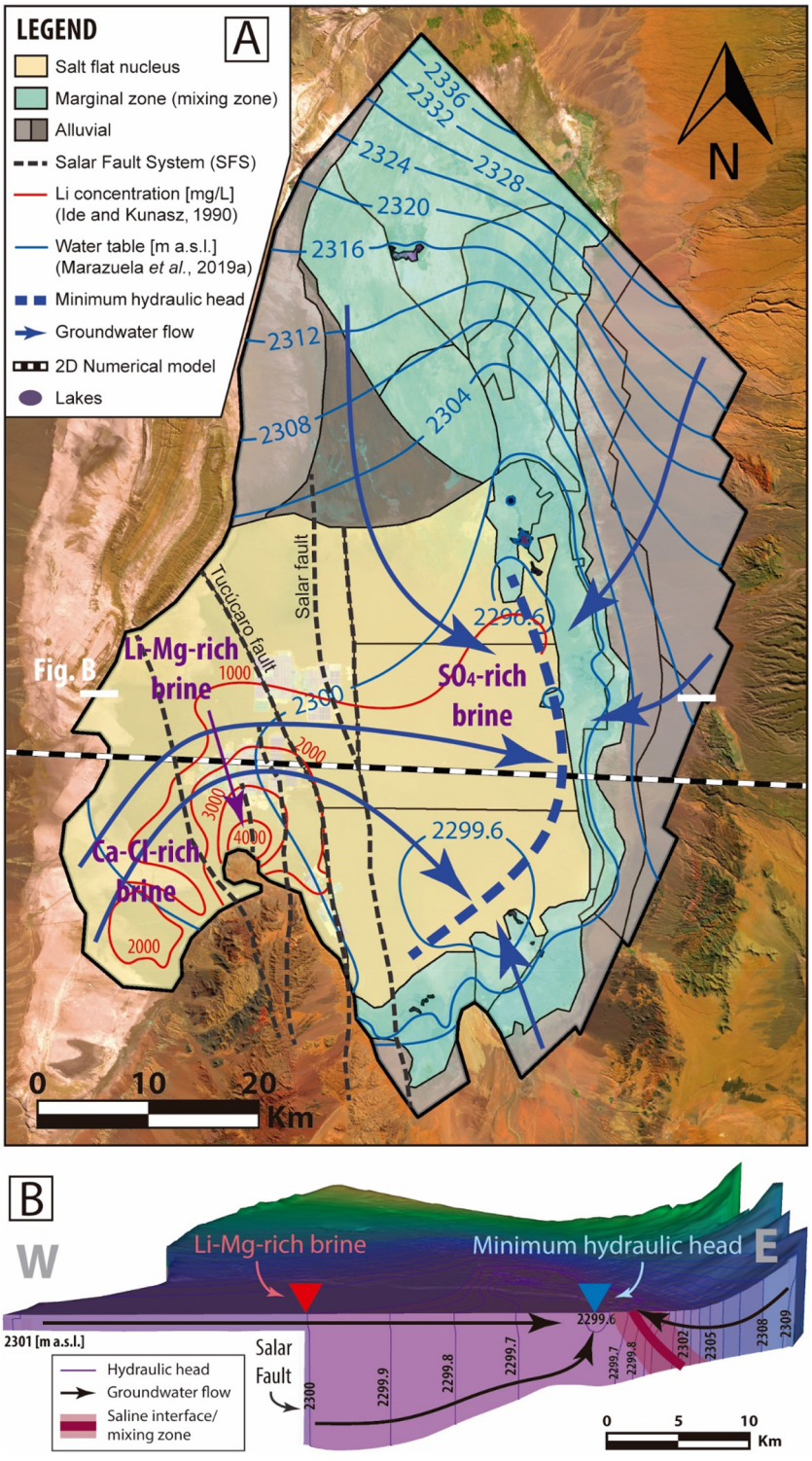

Fig. 2. Hydrogeochemical framework of the Salar de Atacama. A) Water table, types of brines and Li concentration contour map of the sallowest aquifers. Note the spatial mismatch between the minimum hydraulic head of the water table and the Li-Mg-rich brine locations. B) Hydraulic head contour map of the vertical cross-section marked in white in the Fig. A. (Modified from Marazuela et al., 2019a).

et al. (2015) suggested that the basal leakage of evaporated brines from the volcanic arc/Altiplano-Puna active salt flats participated together with meteoric water in the regional groundwater of the southern aquifer feeding the SdA. Using chemical and isotope information of surface and groundwater from the east of SdA and He isotopes in brines, Munk et al. (2018) concluded that more than half of the Li in the halite nucleus is derived from the eastern flank inflows. In order to explain the high Li concentrations from inflow waters to brines, these authors proposed evaporative concentration, transition brines and halite crystallisation. The pending question would be if the water recharged in the eastern flank of the SdA can reach the SFS area and evaporate along its path resulting in Li-rich brines.

An alternative explanation to the Li-Mg-rich brines found in the central-western zone of the nucleus is the ascent of hydrothermal

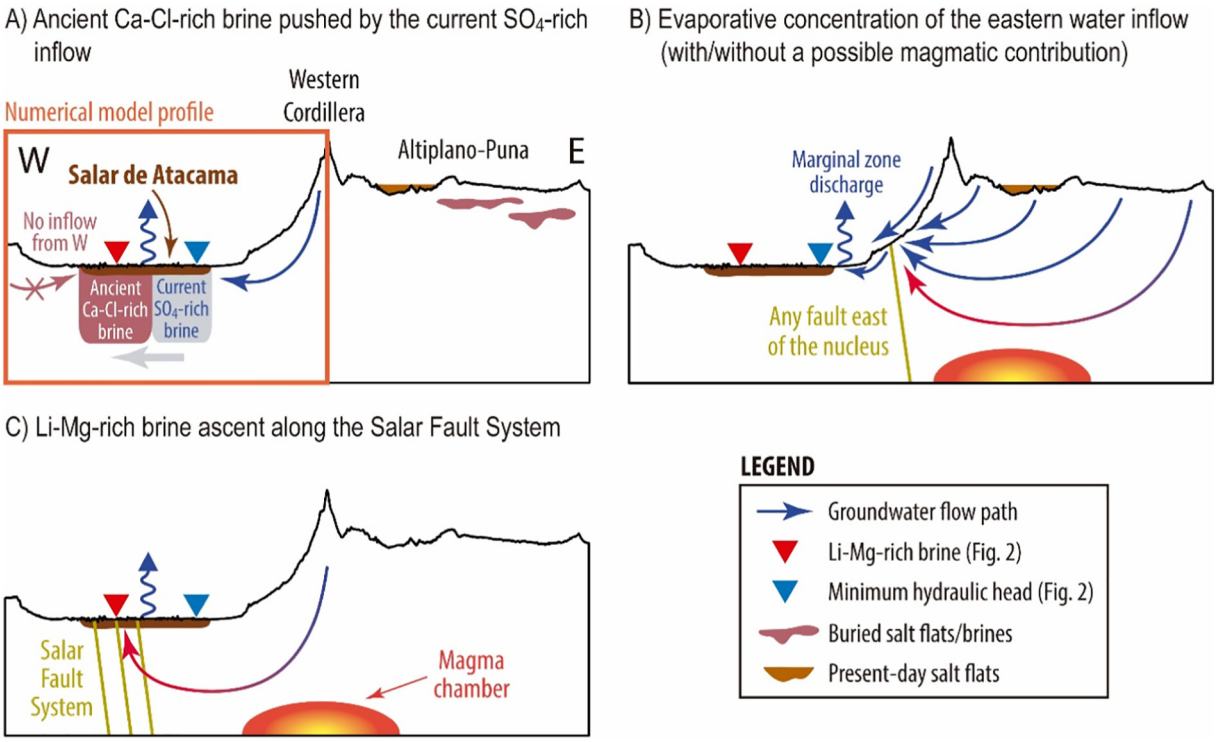

Fig. 3. Conceptual ideas of the Salar de Atacama hydraulic functioning as deduced from the literature: (A) SO_4-rich brines replacing relict Ca-Cl-rich brines, (B) evaporation of the groundwater recharged east of the Salar de Atacama and (C) deep hydrothermal brines ascending along the Salar Fault System. See details in the text.

solutions. Jordan et al. (2002) highlighted the potential hydraulic role of the SFS and suggested that, during desiccated stages, groundwater flow paths coming from the recharge in the eastern flank of the basin could reach the centre of the nucleus and after ascend along the SFS. Following this idea, Lowenstein and Risacher (2009) hypothesized that Ca-Cl-rich deep waters, heated in the subsurface of the volcanic arc at the east of the SdA, rise to the surface of SdA along faults related to the SFS (Fig. 3C). Although no clear genetic link has been established, these Ca-Cl-rich brines coexist with the Li-Mg-rich brines close to the SFS. The ^{3}He isotope values measured by Munk et al. (2016) were interpreted as a possible indicator of the influence of mantle-derived gases. These authors proposed that interaction of groundwater and magmatic systems of the Altiplano-Puna is another potential mechanism for transporting mantle-derived Li, from volcanic systems to the SdA. However, these authors suggested that the fault planes located within the salt flat, such as the SFS, are not good candidates because the lithosphere is cold and rigid (Schurr and Rietbrock, 2004); a better option would be the faults located between the salt flat and the volcanic arc (Fig. 3B). González et al. (2009) related some faults of the SdA basin to deep magma chambers. Lithium contents of approximately 1000 mg/L are common in fluid and melt inclusions associated with volcanic and magmatic rocks (Hofstra et al., 2013; Lindsay, 2001; Schmitt, 2001). The contribution of hydrothermal fluids to the brine compositions has been described in the Salar de Uyuni in Bolivia (Ericksen et al., 1978); the Fox Creek Area in Canada (Eccles and Berhane, 2011); the Salton Sea, Death Valley and Bristol Dry Lake in California (Lowenstein et al., 2016; Lowenstein and Risacher, 2009); the Qaidam basin (Tibet) in China (Li et al., 2018; Lowenstein and Risacher, 2009; Yu et al., 2013); and many other magmatic zones in the world (Benson et al., 2017). Karmanocky and Benison (2016) documented the control of hydrothermal and magmatic pulses on the geochemistry of the Salar Ignorado, located 200 km south of the SdA, through the study of inclusions in gypsum crystals. The study carried out in several salt flats of northwest Argentina by López Steinmetz et al. (2018) confirmed the positive linear correlations between Li, K and Mg, suggesting a common source for these ions, probably a thermal contribution. Again, the hydrogeological connection between the magmatic systems of the volcanic arc and the nucleus of the SdA remains a major pending question.

The previously described conceptual ideas on the genesis of the Li-Mg-rich brines (mainly based on chemistry and isotopic data) hypothesized the evaporation of the water recharged on the eastern flank of the SdA basin (Fig. 3A and B) or the deep groundwater flows in the nucleus from outside the basin (Fig. 3C). However, none of these hypotheses has been tested as feasible by means of groundwater flow numerical models.

The groundwater flow modelling of saline system basins indispensably needs to consider the strong coupling of flow, mass and heat transport and the dependency of density and viscosity on pressure, mass concentration (salinity) and temperature (Driesner and Heinrich, 2007; Klyukin et al., 2016; Kohfahl et al., 2015). In thermohaline systems, the large variations in density and viscosity play an important role in groundwater flow, which is regulated by Darcy's law. Thermohaline convection implies that dense brines counter the upward buoyant flow and convective cells promoted by thermally driven flow (Irvine et al., 2014; Magri et al., 2015, 2012, 2009; Wooding et al., 1997). The leaking of concentrated brines would prevent the salt flats to reach extremely high concentrations (Sanford and Wood, 1991). Furthermore, fault planes are frequently associated with preferential flow paths due to their higher permeability combined with the development of convective cells (Barcelona et al., 2019; Hirthe and Graf, 2015; Koltzer et al., 2017; Li et al., 2016; Magri et al., 2016, 2015, 2010; Shafabakhsh et al., 2019; Simms and Garven, 2004; Zechner et al., 2019). However, although previous work has highlighted the necessity of addressing thermohaline circulation in salt flats (e.g., Godfrey and Álvarez-Amado, 2020; Hardie, 1991, 1990; Magaritz et al., 1990; Munk et al., 2016; Risacher et al., 2003; Rosen, 1994), only synthetic models focused on the saline interface of the shallowest aquifers have been performed to date (Duffy and Al-Hassan, 1988; Fan et al., 1997; Hamann et al., 2015; Holzbecher, 2005; Marazuela et al., 2018; Nield et al., 2008; Simmons et al., 1999; Tejeda et al., 2003; Vásquez et al., 2013). The complexity and high computational cost of these models is probably what

has prevented the development of quantitative thermohaline models that can explain the complex groundwater flow and hydrochemistry of salt flat basins.

The objective of this work is to explain the thermohaline groundwater flow in the Salar de Atacama basin to account for the genesis of the world's largest Li reserve and discuss the feasibility of the hydraulic hypotheses behind all the conceptual genetic models of the Li-rich brines proposed in the literature, in particular, the Li enrichment by evaporative concentration of the inflows feeding the nucleus laterally (Fig. 3A and B) and the ascent of Li-rich hydrothermal brines along the Salar Fault System (Fig. 3C). To achieve this objective a thermohaline numerical model of the groundwater flow has been developed to explain (1) the factors that determine the location of the most evaporated brines within saline systems and (2) how the thermohaline convection in a fractured mature salt flat basin like the present-day Salar de Atacama can contribute to the Li enrichment of brines.

2. Material and methods

2.1. Hydrogeological setting

The SdA basin is a prominent morphological depression of 17,000 km^2 located in the proximal forearc between the Western Cordillera (present-day volcanic arc) to the east and the North Chilean Precordillera (Cordillera de Domeyko) to the west at 2303 m a.s.l. (metres above sea level) (Fig. 1). The SdA basin, especially its eastern flank, is on the arc-shaped region of high heat flow described in the literature between latitudes 15 and 30° south (Hamza et al., 2005). The strong positive anomalies in the isostatic residual gravity of the SdA are caused by dense bodies at 4–6 km and 10–15 km emplaced magmatically or tectonically during the Cretaceous rift episode (González et al., 2009; Reutter et al., 2006).

Successive extensional and compressional regimes have strongly fractured the basin, with the SFS being the best expressed feature (Arriagada et al., 2006) (Fig. 2). The north-northwestern-trending SFS affects the salt flat nucleus from the Cordón de Lila in the south to the Cordillera de la Sal in the northwest, and it has been active over an interval that spans the last 5–10 Ma (Jordan et al., 2007). The SFS has caused the stratigraphic units of the east block of the SdA to be much thicker than those in the west block. At least three other major faults are also described in the literature: the Tucúcaro Fault (which, like the other minor faults in the SdA nucleus, we include in the SFS to simplify the wording), the Peine Fault and a fault referred to in this study as the East Fault (Jordan et al., 2007; Muñoz et al., 2002; Reutter et al., 2006).

The hyper-arid climate of the Atacama Desert, where the SdA is located, was established long before the SdA developed approximately 5.8 Ma ago (González et al., 2009), although some relatively wetter and drier short periods have occurred (Bobst et al., 2001). These climatic cycles have been able to modify the hydrogeological behaviour of the basin over time. Actually, a higher precipitation rate, above 120 mm/yr, occurs in the Western Cordillera flank where elevations above 5000 m a.s.l. are reached (Houston, 2006; Marazuela et al., 2019a). In the salt flat nucleus, the precipitation rate barely reaches 5 mm/yr.

The discharge in the basin occurs mainly by phreatic evaporation in the marginal zone but also minority in the nucleus (Marazuela et al., 2019a, 2019b, 2020). In the marginal zone, where the water table is closest to the ground or directly above the ground in the lakes and wetlands fed by the upward flows of the mixing zone, evaporation rates reach up to 5.84 mm/d (Marazuela et al., 2020). In addition, despite the relatively greater depth of the water table in the nucleus, it also contributes slightly to the discharge in the basin with evaporation rates lower than 0.05 mm/d. Under the current climatic conditions and considering the water table in the shallowest aquifers, the strong asymmetry in the discharge by evaporation seems to prevail over the asymmetry in the recharge, and consequently, the minimum hydraulic head is located in the easternmost zone of the nucleus, close to the marginal zone (Marazuela et al., 2019a, 2019b) (Fig. 2). Therefore, at least in the shallowest aquifers, the recharged water on both flanks of the basin converges towards the eastern part of the nucleus.

2.2. Stratigraphy

The upper crustal lithology and structure of the basin needed to support the modelling works are well known from industry seismic data and a deep exploration well drilled in the centre of the basin (a synthetic profile is shown in Fig. 4) (Jordan et al., 2007; Muñoz et al., 2002; Pananont et al., 2004; Reutter et al., 2006).

The pre-Cretaceous basement is represented by sedimentary and igneous rocks that crop out in the Cordón de Lila peninsula and by widely distributed, stratified volcanic and sedimentary rocks of late Paleozoic to Triassic age. The early Paleozoic rocks are composed of clastic sediments with intercalations of pillow lavas of Ordovician age and Ordovician to Carboniferous plutonic rocks.

The Cretaceous to Eocene sequences that underlie the present-day SdA were deposited in the back-arc of the volcanic arc before 38 Ma

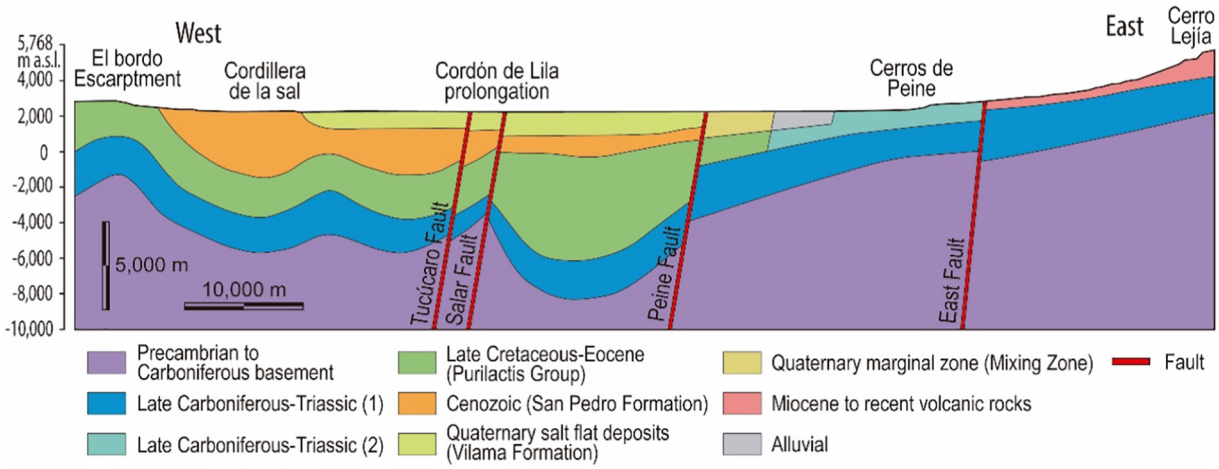

Fig. 4. Simplified stratigraphy and structural features of the vertical profile chosen for the numerical simulations (vertically scaled x1.5 like all profiles shown hereinafter). See the section location in Figs. 1 and 2.

(Reutter et al., 2006). The Purilactis Group (Cretaceous to Eocene) which crops out in the fold and thrust belt of the El Bordo Escarpment, underlies the late Eocene to recent sedimentary fill of the basin. The lowest part of the Purilactis Group is composed of limestones, gypsum and halite, and the upper part is composed of conglomerates. Additionally, basaltic to andesitic lavas, dikes, sills and subvolcanic intrusive rocks were described in these sequences as a consequence of the strong volcanic activity through fissures in the N-S direction.

The Cenozoic rocks correspond to continental clastic sediments and ignimbrites (liparites) associated with substantial extension. The San Pedro Fm. (Eocene-Early Miocene), which crops out in the Cordillera de la Sal, is composed of continental deposits of both clastic (clays, siltstones, sandstones and fine-grained conglomerates) and evaporitic (halite and gypsum precipitated in an ancient tertiary salt flat) rocks. The equivalent Tambores Fm. is composed of paraconglomerates and poorly consolidated sandstones.

The Quaternary is mainly represented by the Vilama Fm. (late Pliocene-present), which constitutes the SdA halite nucleus. The dating of the five ignimbrite layers originally expelled from the volcanic arc (stratovolcanoes) and currently buried in the Vilama Fm. constrain the age of the nucleus deposits to 5.8 Ma (De Silva, 1989; Gardeweg and Ramírez, 1987; González et al., 2009).

2.3. Numerical model

The thermohaline flow modelling encompassed three numerical simulations based on the geological profile shown in Fig. 4, and whose main characteristics are summarized in Table 1. The first two simulations (symmetric and asymmetric simulations) aimed to analyse the effect of the evaporation discharge distribution across the salt flat surface on the location of the most evaporated brines and, therefore, of the expected Li-Mg-rich brine if only evaporation was considered as mechanism of Li enrichment. The third simulation (mature stage simulation) reproduced the current hydraulic conditions of the SdA basin to characterize its thermohaline groundwater flow and search for a numerically validated hypothesis of the genesis of Li-Mg-rich brines.

2.3.1. Coupled formulation

The FEFLOW code (Diersch, 2014; Shao et al., 2016) was used to model the strong coupling of groundwater flow, solute transport and heat transfer based on the following governing equations.

The equation of fluid mass conservation in equivalent hydraulic heads is defined as:

$$S_s\frac{\partial h}{\partial t}+\nabla\cdot\mathbf{q}=0 \tag{1}$$

where S_s is the specific storage, h is the equivalent hydraulic head and $\mathbf{q}$ is Darcy's law, which describes the flow of a fluid through a porous medium:

$$\mathbf{q}=-\mathbf{K}\left[\nabla h+\frac{\rho^f-\rho_0^f}{\rho_0^f}\mathbf{u}\right] \tag{2}$$

where $\mathbf{K}$ is the hydraulic conductivity tensor, ρ^f is the fluid density and ρ_0^f is the reference density. The second added term of this law is the product of the density ratio and the gravitational unit vector, $\mathbf{u}$, which represents the buoyancy force induced by density variations.

The energy-balance equation for the fluid and porous medium is given by the expression:

$$\frac{\partial}{\partial t}\Big(\left(\phi\rho^f c^f+(1-\phi)\rho^s c^s\right)T\Big)+\nabla\cdot\left(-\boldsymbol{\lambda}\nabla T+\rho^f c^f T\mathbf{q}\right)=0 \tag{3}$$

where ϕ denotes the porosity, ρ^s is the density of the solid, T is the temperature, c^f is the specific heat of the fluid, c^s is the specific heat of the solid and $\boldsymbol{\lambda}$ is the thermal conductivity of the saturated porous medium as a whole.

The equation of solute-mass conservation in its convective form is as follows:

$$\phi\frac{\partial C}{\partial t}+\mathbf{q}\cdot\nabla C-\nabla\cdot(\mathbf{D}\nabla C)=0 \tag{4}$$

where C is the mass concentration and $\mathbf{D}$ is the tensor of hydrodynamic dispersion.

The tensor of hydraulic conductivity, $\mathbf{K}$, is defined as:

$$\mathbf{K}=\frac{\mathbf{k}\rho_0^f g}{\mu^f} \tag{5}$$

where $\mathbf{k}$ is the intrinsic permeability tensor. The dynamic viscosity of the fluid phase, μ^f, is regarded as a thermodynamic function of mass fraction, ω, and T. The pressure (p) dependence on brine viscosity can be neglected at subcritical temperature (Schoofs and Hansen, 2000). Combining the high-concentration dependency given by Lever and Jackson (1985) with the empirical temperature dependency of Mercer and Pinder (1974), the following expression is reached employing reference values for concentration, C_0, and temperature, T_0:

$$\mu^f(C,T)=\mu_0\frac{1+1.85\omega-4.1\omega^2+44.5\omega^3}{1+1.85\omega_{(C=C_0)}-4.1\omega^2_{(C=C_0)}+44.5\omega^3_{(C=C_0)}}\frac{1+0.7063\varsigma_{(T=T_0)}-0.04832\varsigma^3_{(T=T_0)}}{1+0.7063\varsigma-0.04832\varsigma^3} \tag{6}$$

where $\varsigma=(T-150)/100$ at T in °C and $\omega=C/\rho^f$.

The equation of state used for the fluid density is given in terms of reference values for density, concentration, temperature and pressure, p_0, by the *BrineDensity* plug-in implemented in the FEFLOW code (Magri, 2009):

$$\rho^f(C,T,p)=\rho_0^f\left(1-\overline{\beta}(T-T_0)+\overline{\gamma}(p-p_0)+\frac{\overline{\alpha}}{C_s-C_0}(C-C_0)\right) \tag{7}$$

where the coefficients of thermal expansion, , compressibility, , and mass concentration ratio, , vary as a function of C, T and p.

2.3.2. Mesh and model parameters

The 2D model extended from west to east across the basin and reached the Precambrian-Carboniferous basement throughout (Figs. 1 and 4). The 2D model represented a selected section quite parallel to the main groundwater flow and, therefore, out-of-plane groundwater contributions were neglected as a simplification (Fig. 2). The objective of this model was not to calibrate field data (there are no data at depth) but to describe thermohaline hydrodynamics at basin scale. This section captured the main hydrodynamic features that constitute the basis of the discussion, such as the developing of a mixing zone around the salt flat nucleus, the hydraulic role of the minimum hydraulic head of the regional water table and the possible convective flow in the SFS. All of them proved to be intrinsic to saline systems and, therefore, although their location or geometry can vary depending on the hydraulic parameters and recharge/discharge ratio, the regional hydraulic behaviour that they trigger does not change.

The maximum elevation was reached at the eastern boundary (Cerro Lejia) with 5769 m a.s.l. On the other side, the profile only reaches an elevation 2871 m a.s.l. at the Border Escarpment. The salt flat nucleus was located 2303 m a.s.l. at the centre of the profile. Due to the syncline-shaped basin, the Precambrian-Carboniferous basement was reached 8300 m b.s.l. (metres below sea level) beneath the nucleus and only 2200 m a.s.l. below the volcanic arc.

The finite-element mesh was built using the "Triangle" algorithm and satisfying the Delaunay criterion (Shewchuk, 1996). The whole profile comprised approximately 120,000 triangular elements. The element

Table 1
Summary of the main characteristics of the three thermohaline simulation carried out in this work. E: evaporation.

Simulation	Time	Objective	Specific considerations
Symmetric evaporation	100,000 yr	Location of the most evaporated brines in a hypothetical ancient salt flat with symmetric evaporation	$E_{nucleus} = E_{marginal\ zone}$ Faults disabled
Asymmetric evaporation		Location of the most evaporated brines in a salt flat with asymmetric evaporation	$E_{nucleus} < E_{marginal\ zone}$ Faults disabled
Mature stage	Quasi-steady-state	Thermohaline flow in the present-day Salar de Atacama basin	$E_{nucleus} < E_{marginal\ zone}$ Pore water of San Pedro and Vilama Fms. is saturated in halite

size ranged from approximately 25 m in the faults and evaporation zones, which allowed implementing the evaporation boundary conditions in the nucleus and marginal zone as described below, to an average value of 150 m in the less critical areas to avoid numerical errors.

Faults were represented as permeable areas of 300 m width (it was very small compared to the basin-scale groundwater flow) extending from the basement to the top of the model, using the well-established equivalent porous media (EPM) approach (Blessent et al., 2014; Vujević et al., 2014). The EPM technique requires less computational effort than discrete-fracture models and it allows modeling the density-driven flow inside the faults (Magri et al., 2016, 2015, 2012, 2010). Faults were disabled in the symmetric and asymmetric evaporation simulations.

Each stratigraphic unit was considered homogeneous and isotropic with respect to the physical properties (hydraulic conductivity, porosity, thermal conductivity and volumetric heat capacity) listed in Table 2. Average values of each parameter were taken from previous studies in the SdA (e.g., Marazuela et al., 2019a, 2019b) and complemented with literature reference values for each type of rock (e.g., Eppelbaum et al., 2014). The basement was considered impermeable and then neglected in the modelling task. Due to its extremely low hydraulic conductivity, preliminary simulations demonstrated that neglecting the basement did not have a significant impact on the groundwater flow. The longitudinal and transverse dispersivities for both, mass and heat transport, were 100 and 10 m, respectively.

Owing to the chemical equilibrium of the brines with halite in most of the system considered, the impact of dissolution-precipitation on porosity and permeability is expected to be small at basin-scale and, therefore, it has been neglected. Although a fully coupled thermohaline reactive transport model has been partially attempted at local and simpler scale (e.g. Graf and Therrien, 2007), the computational cost of such model at basin-scale is far beyond the current conventional computational resources and is often despised (e.g., Magri et al., 2015, 2009; Zechner et al., 2019).

2.3.3. Boundary and initial conditions

Groundwater flow and mass transport boundary conditions (BCs) encompassed freshwater inflow along the recharge areas on the eastern and western flanks of the basin and a freshwater sink in the nucleus and marginal zone (Fig. 5). The inflow rate was based on the recharge values presented by Marazuela et al. (2019a). The main recharge occurred on the eastern flank, with values that increase from 34 mm/yr in the contact between the alluvial deposits and the outcropping Triassic rocks to 85 mm/yr in Cerro Lejía. These values correspond to the current rainfall rates of 40 to 100 mm/yr minus the 15% that is estimated by interception, surface detention and infiltration at the beginning of a storm and that finally back to the atmosphere through evaporation. On the western flank, the recharge was reduced to 5.5 mm/yr. These inflow rates led to a total recharge of 5.7 m^3/d. As a requirement for numerical calculation, the hydraulic head was fixed at 5000 m a.s.l. at the easternmost node of the top to allow the free calculation of the water table in the centre of the basin, where the salt flat and mixing zone are located. Both freshwater inflows (with the exception of the San Pedro Fm. stretch in the mature stage simulation, as described below) had a concentration of 5000 mg/L, which represented a recharge water slightly enriched in solutes after having passed through volcanic rocks.

The evaporation was implemented as a freshwater sink across two rectangles 200 m wide that extends along the top of the nucleus and marginal zone. This sink allowed the extraction of pure freshwater (0 mg/L) without solutes, thereby increasing the solute concentration in each consecutive time step through evaporative concentration (Nield et al., 2008). For the asymmetric evaporation and mature stage simulations that considered the present-day evaporation, the outflow in the nucleus and marginal zone was 0.3 and 5.4 m^3/d, respectively, in accordance with the evaporation rates estimated by Marazuela et al. (2020) (Fig. 5). For the symmetric evaporation simulation that considered a homogeneous evaporation rate across the entire surface (nucleus and marginal zone), the total outflow also remained at 5.7 m^3/d. Therefore, in all simulations the water inflows and outflows were compensated (closed basin). The normalization range for concentration was established between 0 mg/L, equivalent to pure freshwater with a density of 1000 kg/m^3 and 350,000 mg/L with a density of 1200 kg/m^3. For the mature stage simulation, the groundwater of the San Pedro and Vilama Fms. was assumed to have the maximum solute concentration (350,000 mg/L), representing the rapid attainment of halite saturation by dissolution of their evaporitic rocks. Additionally, a mass concentration BC limited the maximum concentration (350,000 mg/L, which corresponds to halite saturation) that the brine could reach in each node of the evaporation rectangle (Kohfahl et al., 2015).

The heat transport BC allowed reproducing the geothermal gradient considering the heat flow values obtained by Hamza et al. (2005). The heat inflow at the bottom increased from 80 mW/m^2 at the eastern end to 120 mW/m^2 at the western end, taking into account that the crust below the salt flat nucleus is colder than that below the volcanic arc (Fig. 5). An average atmospheric temperature of 18 °C was fixed at the top of the model. The lateral boundaries were closed to fluid, heat and mass flow because they were considered the limits of the basin. Also the bottom was closed to fluid and mass flow.

The initial conditions for hydraulic head and temperature were derived from a convective hydrothermal model that was previously carried out. The initial mass concentration was 5000 mg/L in the entire domain, representing a hypothetical basin filled completely with recharge freshwater. The mature stage simulation was run until the quasi-steady state regime was achieved.

3. Results

3.1. Solute enrichment by evaporation in salt flats

Although prior to a salt flat development, the SdA basin was probably occupied by a freshwater lake governed by a topography-driven flow, this initial flow regime changed drastically when the freshwater lake evolved to a salt flat and the increase in solute concentration modified the density of the groundwater. During its stage as saline system (at least from 5.8 Ma ago), there are two possible hydraulic regimes through which the basin has been able to evolve or alternate and which must be analysed for its possible implication in the solute enrichment process. These regimes are: (1) salt flat with homogenous

Table 2
Hydraulic and thermal parameters considered for the numerical simulations. The colours are in accordance with the geological profile shown in Fig. 4.

Hydrostratigraphic units	K [m d^{-1}]	ϕ [–]	λ [W m^{-1} °C^{-1}]	$\rho^s c^s$ [10^6 J m^{-3} °C^{-1}]
Precambrian to Carboniferous basement	Impermeable			
Late Carboniferous-Triassic (1)	$5{\cdot}10^{-4}$	0.02	2.8	2.1
Late Carboniferous-Triassic (2)	$2{\cdot}10^{-2}$	0.02	2.8	2.1
Late Cretaceous-Eocene	$1{\cdot}10^{-3}$	0.03	2.6	2.1
Cenozoic	$1{\cdot}10^{-2}$	0.04	3.0	2.0
Quaternary salt flat deposits	0.1	0.02	3.5	1.8
Evaporation zone of the nucleus	0.5	0.05	3.5	1.8
Quaternary marginal zone	0.1	0.02	3.2	1.8
Evaporation zone of the marginal zone	0.5	0.05	3.2	1.8
Miocene to recent volcanic rocks	1	0.10	2.8	2.1
Alluvial	2	0.10	1.8	1.7
Faults (EPM)	1	0.25	2.0	1.8
Fluid	–	–	0.65	4.2

evaporation throughout the salt flat surface (called here symmetric evaporation) and (2) salt flat with asymmetric evaporation like the present-day SdA. In this section, two numerical simulations was carried out to analyse the effect of considering a symmetric or asymmetric evaporation distribution across the salt flat surface on the location of the most solute enriched brines by evaporative concentration.

The results showed that, assuming a symmetric evaporation rate on a hypothetical ancient salt flat, the minimum hydraulic head of the regional water table was computed in the western nucleus as a consequence of the present-day asymmetry in the recharge (Fig. 6). The minimum hydraulic head determined the direction towards which the most evaporated brine tended to move and accumulate; therefore, it had capital significance for the enrichment of Li and other conservative elements in the brine and for the precipitation of salts. The groundwater coming from the recharge in the mountains was increasing its concentration in solutes by evaporation and accumulated at the minimum hydraulic head, forming a "salt bulge". The density contrast generated by the solute concentration gradient led the system to convection and, thus, the brackish water began to sink due to its higher density. The salt bulge evolved downwards until it reached the impermeable basement. Although the sinking process was sensitive to the hydraulic parameters of the rocks, and low permeability layers slightly favoured its lateral expansion, the reaching of the basement by the salt bulge in forming occurred even before saturation in halite was achieved in the shallowest layers (Fig. 6B). That is, the leakage of evaporated brine from the salt flat towards deep layers was favoured with respect to lateral expansion even when the rocks had low permeability. This occurred because the density gradient was very strong and the density-driven flow overcame the topography-driven flow. In addition, the effect of temperature gradient on brine density enhanced this deepening. When the present-day asymmetric evaporation was considered, the minimum hydraulic head moved towards the contact between the nucleus and the eastern marginal zone (Fig. 7). The following evolution of the salt bulge was similar to that described for the symmetric evaporation regime. Therefore, symmetric or asymmetric evaporation significantly affected the location of the most evaporated brines.

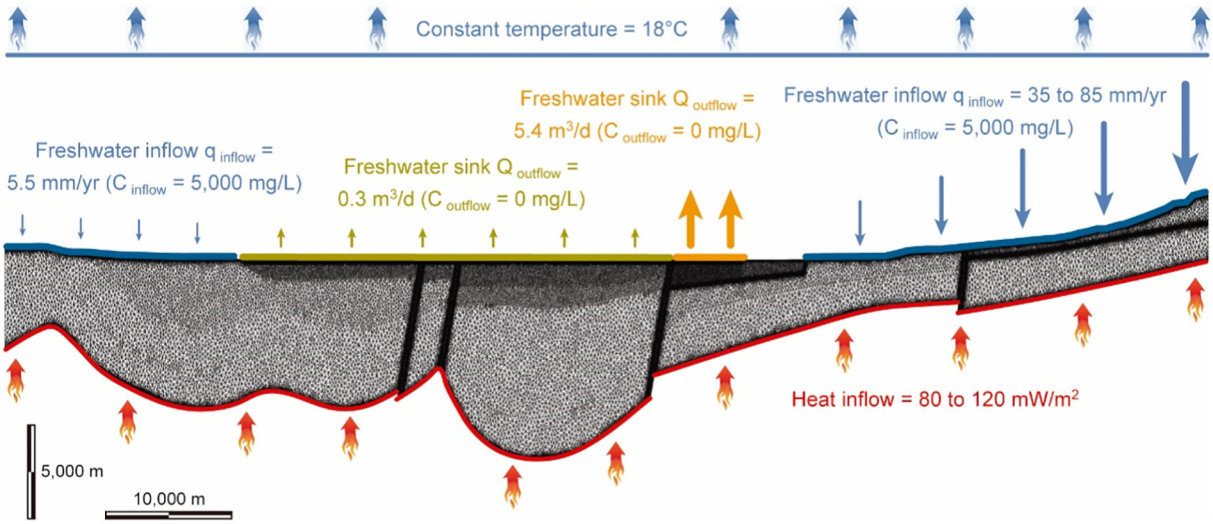

Fig. 5. Mesh and sketch of the main flow, mass and heat boundary conditions considered for the numerical model. Note that the freshwater sink shown correspond to the present-day asymmetric distribution of the evaporation; for the symmetric evaporation simulation, the total freshwater sink remained at 5.7 m^3/d with a constant distribution of it across the nucleus and marginal zone. See details in the text for the consideration of San Pedro and Vilama Fms. as a saline domain.

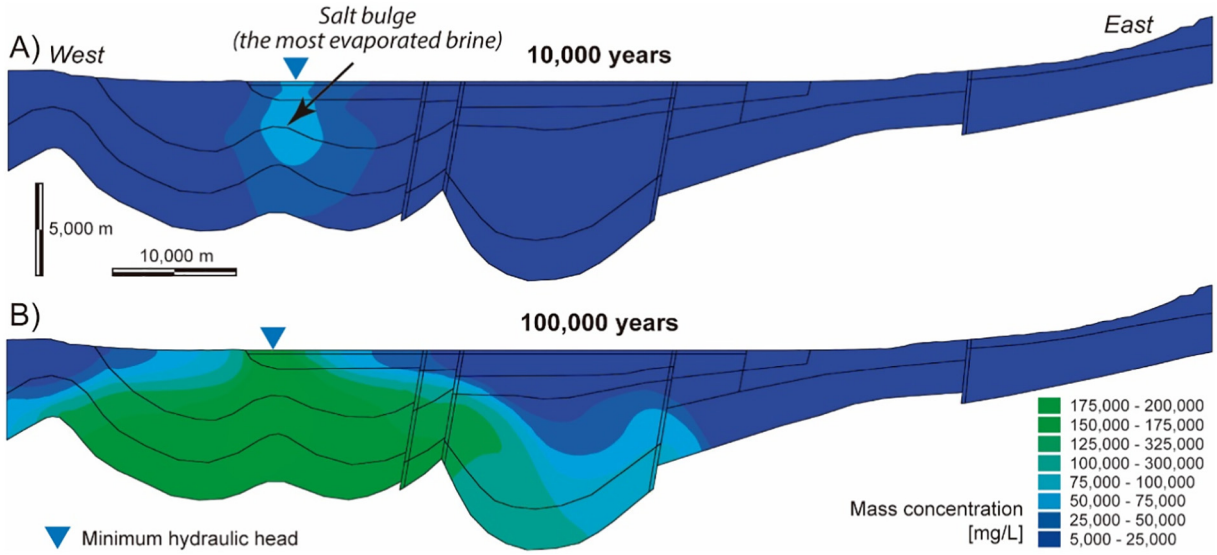

Fig. 6. Computed mass concentration as resulted from the symmetric evaporation simulation. The brines produced by evaporative concentration accumulate at the minimum hydraulic head (salt bulge), which is located in the western edge of the salt flat nucleus.

In addition, because the brine preferably sinks instead of expanding laterally, reaching the width of the current SdA nucleus only by evaporation seems unlikely. The model results suggest that, although it cannot be completely ruled out, evaporation alone would take too long to fill the SdA nucleus (Figs. 6B and 7B). The dissolution of salt rocks belonging to San Pedro and Vilama Fms., as it is considered below for the mature stage simulation, could contribute to explain this fact.

3.2. Thermohaline circulation in the Salar de Atacama

The results of the mature stage simulation showed the effects of temperature and salinity on the groundwater flow of the SdA basin (Fig. 8). The temperature gradients predicted by the model below the SdA, 25 °C/km, and below the Western Cordillera, 35 °C/km, were consistent with the 18–31 °C/km obtained by Jayne et al. (2016) for the Salar de Huasco located farther to the north (Fig. 8A). These results confirmed that the lithosphere is cooler in the central part of the basin than in the volcanic arc, although this did not prevent convection. The computed temperature field was constrained by the syncline-shape geometry of the basin, which determined the distribution of the hydraulic and thermal parameters. The temperature field also was distorted by the presence of faults and the saline interface.

In the mature stage, a saline interface and its associated mixing zone were located around the salt flat nucleus as a consequence of the density contrast generated by the mass concentration gradient between the brine in the nucleus and the recharged freshwater in the mountains (Fig. 8B and C). The geometry of the mixing zone was controlled by the ratio between the freshwater recharge and the evaporation discharge and by the hydraulic parameters of the basin rocks. Thus, the slope of the eastern mixing zone close to the surface was lower than at depth (Fig. 8D). Marazuela et al. (2018) already pointed out that the presence of highly permeable rocks in the shallowest aquifers results in a slope of the mixing zone much lower than previously predicted in the SdA.

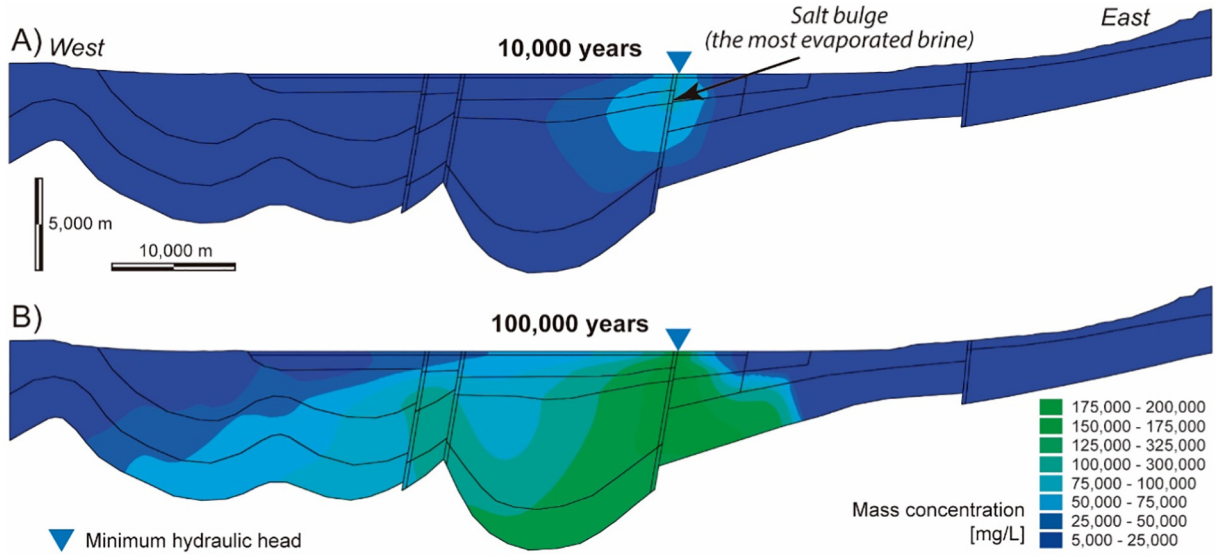

Fig. 7. Computed mass concentration as resulted from the asymmetric evaporation simulation. The salt bulge produced by accumulation of evaporated brines is located in the eastern edge of the salt flat nucleus, where the minimum hydraulic head is computed. Note that at 100,000 years, the width of the salt bulge is still far from the width of the present-day Salar de Atacama nucleus because the brine preferably sinks instead of expanding laterally.

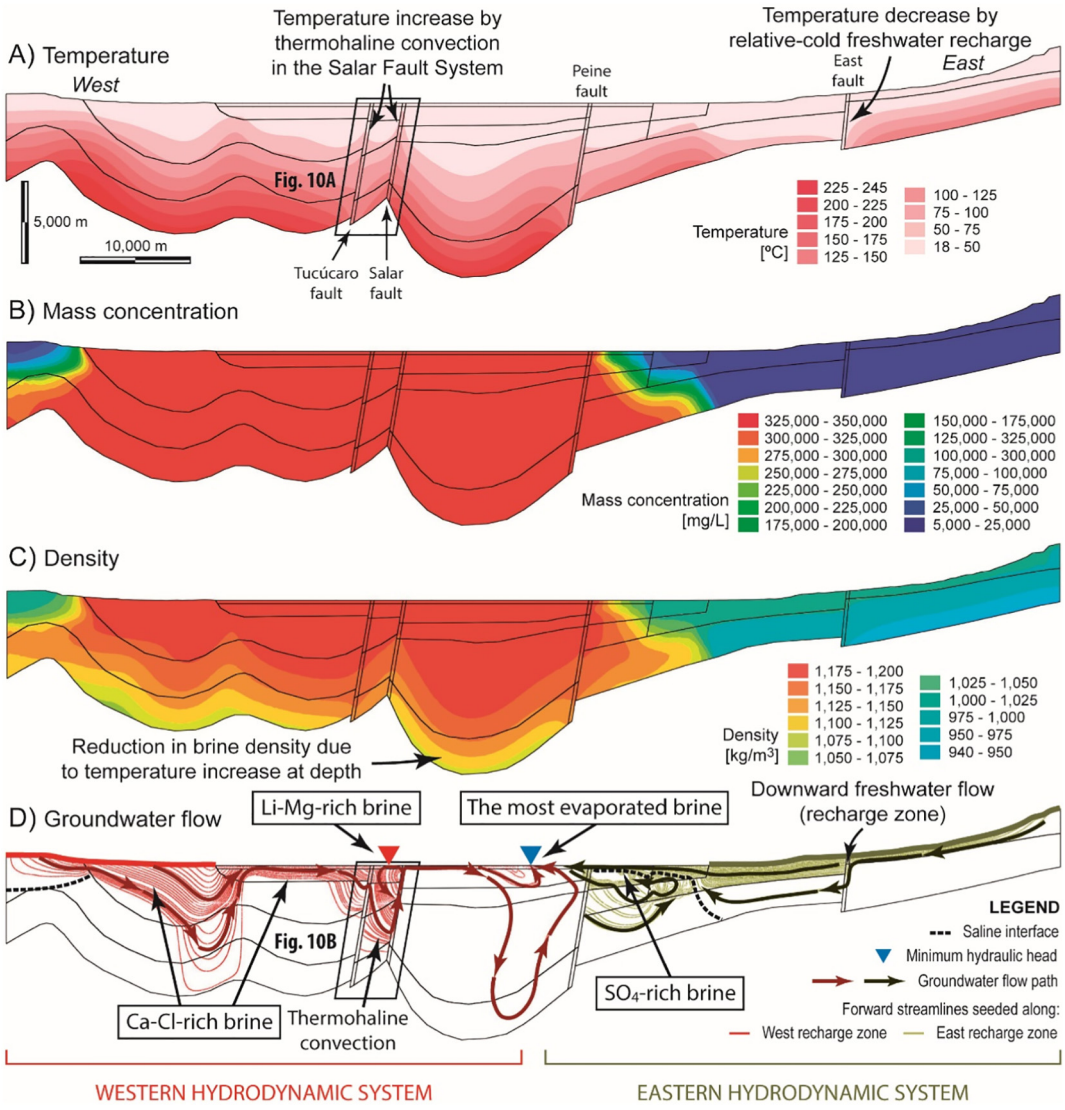

Fig. 8. Computed (A) temperature field, (B) mass concentration, (C) density and groundwater flow (D) as resulted from the mature stage simulation. The Salar Fault System showed in Fig. 10 is framed with two black parallelepipeds.

Because of the increase in temperature with depth, the density of the brine below the nucleus decreased from 1200 to 1100 kg/m^3 (Fig. 8C). This reduction in density favoured the brine leakage from the bottom of the salt flat and the subsequent lateral entry of relatively more dilute fluids at the top. As the precipitation of salts would only occur when saturation in halite was reached, this explains why the porosity and permeability of the shallow aquifers do not decrease dramatically due to salt precipitation.

However, despite this density reduction, the mixing zone did not disappear at depth (Fig. 8B and C). The persistence of the mixing zone at depth was a critical factor for basin-scale hydrodynamics because it prevented any groundwater flow path coming from the recharge zone in the Western Cordillera, or hypothetically in the Altiplano-Puna, directly reaching the SFS in the nucleus. This did not rule out a possible groundwater contribution from the Altiplano-Puna to the SdA basin, but any flow path coming from this region would be forced to ascend to the marginal zone before joining the nucleus.

At basin-scale, a key factor was that the minimum hydraulic head of the regional water table divided the system into two isolated hydrodynamic systems, eastern and western (Fig. 8D). The minimum hydraulic head was computed in the easternmost part of the salt flat nucleus, close to the eastern mixing zone. In this location, the flow paths coming from both hydrodynamic systems converged and terminated.

In the eastern hydrodynamic system, the groundwater recharged in the mountains moved along shallow aquifers, but when it reached highly permeable faults like the East Fault, the flow path descended (Fig. 8D). Due to the downward direction of the relatively cold flow in the fault, a negative anomaly in the temperature field was produced (Fig. 8A). Finally, the freshwater coming from the Western Cordillera was forced to flow upward to the surface of the marginal zone by the mixing zone, feeding the wetland and lake ecosystems in the area (Figs. 8D and 9). The flow paths became almost parallel to the surface in the shallowest aquifers of the marginal zone due to the very low slope of the mixing zone described above. That is where the highest flow rates of the system occur, at peak velocity of 7 m/yr (Fig. 9). Along this quasi-horizontal flow path, the shallow water table experienced intense evaporation, resulting in a rapid increase in the solute concentration and leading the fluid to halite saturation before it reached the minimum hydraulic head. The low flow that reached the nucleus did not surpass the point of the minimum hydraulic head and, as a consequence, it recirculated by convection along the inner side of the mixing zone.

In the western hydrodynamic system, the rapid attainment of halite saturation by the scarce recharge was likely due to the geology of the area. As described in Section 2.2, evaporitic rocks crops out throughout the western margin of the salt flat through the Cordillera de la Sal and extends deep below the entire salt flat (Arriagada et al., 2006; Jordan et al., 2007). Conceptualization of the San Pedro and Vilama Fms. as a saline domain in which pore water is saturated in halite led to a brine of homogeneous density throughout the entire salt flat nucleus (Fig. 8C). Previous simulations that did not consider the San Pedro and Vilama Fms. as a saline domain demonstrated that the computed location of the minimum hydraulic head and the regional flow pattern did not change significantly, and only the width of the salt flat nucleus was reduced. The assumption of the leaching of the water-soluble rocks from the Cordillera de la Sal implied that the groundwater entering through the western margin of the nucleus was a brine with a density of 1200 kg/m^3. The brine coming from the west moved towards the minimum hydraulic head in the easternmost zone of the nucleus and along this path a weak evaporation occurred. The groundwater flow inside the nucleus featured a very low velocity due to the small hydraulic gradients induced by its flat topography.

Also, during its crossing towards the minimum hydraulic head in the easternmost zone of the nucleus, some brine was captured by the convective flow developed in the SFS (Fig. 8D). The computed groundwater flow indicated that complex thermohaline circulation occurred in the SFS (Fig. 10). The density contrast induced by temperature and salinity gradients was the driving force of this thermohaline circulation (Fig. 10A). Internal convection cells developed not only around the faults but also inside the faults, similar to those described in other thermohaline systems (Magri et al., 2012, 2010) (Fig. 10B). Convection circulated groundwater inside the SFS at velocities ranging between 0.25 and 2.5 mm/yr, which was one to three orders of magnitude higher than in the surrounding rocks. This deformed the temperature field, with a temperature decrease on the eastern side of the Tucúcaro Fault and western side of the Salar Fault and an increase on the opposite sides of these faults (Fig. 10A). The thermohaline convection in the SFS could notably favour the remobilization of solutes, such as Li or Mg, that were hypothetically contained in the mineral structures of deep layers of salts and/or clays.

4. Discussion

4.1. The minimum hydraulic head constraint

According to the modelling results, the minimum hydraulic head determines the direction in which the most evaporated brines tend to converge and accumulate (Figs. 6, 7 and 8). Therefore, the most evaporated brines in salt flats are expected at the minimum hydraulic head. As the highest concentration of Li is found in the SFS in the central-western nucleus (Fig. 2), the present-day minimum hydraulic head should be located in that area to explain the Li enrichment as a result of evaporative concentration. But only if the evaporation was homogeneous across the entire surface of the salt flat (symmetric evaporation) would the minimum hydraulic head be located in the central-western portion of the nucleus (Fig. 6). This hypothetical scenario could have occurred in previous stages of the SdA formation and it is possible that layers buried today under the current salt flat recorded this old hydraulic regime. Therefore, it is likely that deep layers have the maximum lithium concentration in the SFS area. However, despite the low topography-driven flow in the nucleus and due to the high hydraulic conductivity of its shallowest aquifers, the current brine hydrochemistry of the shallowest aquifers has to be consistent with the current groundwater flow. In recent times, the minimum hydraulic head is located in the easternmost zone of the nucleus (Figs. 2 and 8D), which implies that the most evaporated brines are also expected in the easternmost zone of the nucleus and not in the SFS. Thus, it is not possible to explain the Li-Mg-rich brines in the SFS only by evaporative concentration of the inflows coming from the eastern flank as the hypotheses of Fig. 3A and B would require.

4.2. The mixing zone as a regional hydraulic barrier for deep groundwater flow

In the eastern hydrodynamic system, the development of a mixing zone surrounding the salt flat nucleus causes the less dense recharge to float on and partially mix with the dense brine occupying the nucleus of the salt flat (e.g. Fan et al., 1997) (Figs. 8D and 9). The abundance of native sulfur in the volcanoes of the Western Cordillera leads to SO_4-rich inflow waters (Risacher et al., 2003). After evaporative concentration in the marginal zone, SO_4-rich brines are produced. These SO_4-rich brines accumulate in the east block of the nucleus, since the minimum hydraulic head prevents its advance towards the west block (Fig. 9).

The computed thermohaline circulation showed that, although it may be slightly distorted by the temperature gradient, the eastern mixing zone continues downward to the lower impermeable boundary (Fig. 8). The persistence of the mixing zone at depth has important implications for the regional hydrodynamics of the basin because it forces any deep groundwater flow path coming from the east to ascend to the marginal zone surface. This prevents any deep hydrothermal fluid heated below the volcanic arc to reach and ascend along the SFS as the hypothesis of Fig. 3C would require. Therefore, if the majority origin of Li was anywhere to the east of the mixing zone (including the

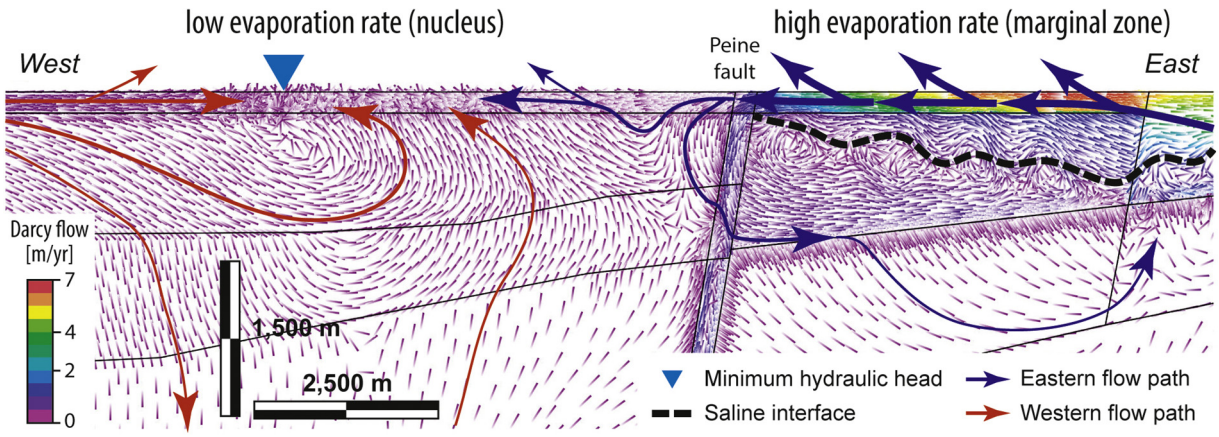

Fig. 9. Darcy flow and groundwater flow streamlines of the marginal zone and eastern salt flat nucleus. The flow path coming from the eastern recharge zone is forced to rise to the surface by the mixing zone, and close to the surface is strongly evaporated producing a SO_4-rich inflow brine. In addition, the flow paths coming from opposite recharge zones converge at the minimum hydraulic head, where the most evaporated brines are expected.

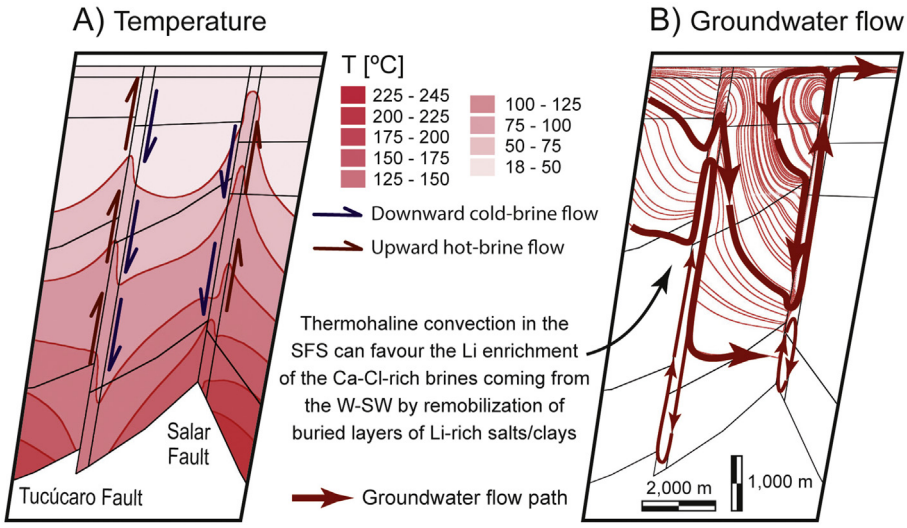

Fig. 10. Computed (A) temperature field and (B) groundwater flow in the Salar Fault System as resulted from the mature stage simulation. The location of the figures is shown in Fig. 8.

Altiplano-Puna) the highest concentration of Li would be located in the easternmost zone of the nucleus, where the minimum hydraulic head of the water table is located and the flow paths terminate.

4.3. The role of fractures and thermohaline convection in the formation of Li-rich brines

The location of the Li-Mg-rich brines in the SFS suggests that fractures could have played an active role in the accumulation of Li and Mg. A key question to discuss, therefore, is the origin of the hypothetically Li-Mg-enriched solution that ascends along the SFS. Hereafter, we propose that the extreme enrichment in Li can be explained as a result of the remobilization of an ancient deposit of Li-Mg-enriched salts or clays located below the present-day salt flat nucleus. This enrichment could form under ancient hyper-arid climatic conditions and homogeneous evaporation. Then, the minimum hydraulic head was computed in the western nucleus as a consequence of asymmetry in the recharge (Fig. 6).

In the western hydrodynamic system, the water recharged on the Cordillera Domeyko and the Cordillera de la Sal quickly increases in density by dissolution of salts in the San Pedro Fm. This produces Ca-Cl-rich inflow brines similar to the described by Risacher and Alonso (1996), although still poor in Li and Mg. Besides the Ca-Cl-rich brine produced by the dissolution of the San Pedro Fm. at the west of the nucleus, some inflows out-of-plain coming from the southwest boundary of the nucleus (as the water table of the Fig. 2 suggests) could mix with the Ca-Cl-rich brines in the southwestern zone of the nucleus previously to incorporate in the SFS.

Once incorporated to the nucleus, the brines move towards the minimum hydraulic head at the east of the nucleus (Fig. 8D). However, the presence of the SFS can capture these brines and incorporate them into its complex thermohaline convection (Fig. 10). In accordance with the model results, the western brine tends to sink several hundred or thousands of metres along the Tucúcaro Fault and then return to the shallowest aquifer of the salt flat along the Salar Fault due to convective circulation. Along this flow path, the brine could be enriched in Li and other solutes if a layer of old salt or exchangeable-position clay enriched in these elements exists in depth. The enrichment in Li and Mg would cause the precipitation of some halite together with a small increase in the density of the brine which have not been considered in the calculations. Finally, the Li-Mg-rich brine resulting from the remobilization of Li and Mg moves towards de minimum hydraulic head where it converges with the SO_4-rich brine (Figs. 8D and 9). In addition, the diffusion and dispersion processes do not considered by the streamline representations of the Fig. 8D contribute to the mixing of brines leading to smooth transitions between them across the nucleus. Similarly, the δ^2H and $\delta^{18}O$ values of the subsurface brine in the Salar del Hombre Muerto plotted along the meteoric water line, suggested the inflow of deep dilute water with salt from halite dissolution (Godfrey et al., 2013).

The existence of Li salts as a source of Li has never been reported in the geological record of evaporites in the Central Andes (Risacher and Fritz, 2009). Indeed, although K, Mg and B are known to accumulate in soluble salts (chlorides, sulfates and borates) under advanced evaporation stages, Li cannot enter the crystalline structures of the salts, and the majority remains in the liquid phase (Garrett, 2004; Pueyo et al., 2017; Song et al., 2017). Thus, to precipitate as LiCl, the brine must evaporate up to 38% w/w LiCl, beyond the formation of sylvite, carnallite and bischofite (Garrett, 2004). The existence of Li-rich clays has been, however, more commonly reported. For example, hectorite, which forms from the alteration of rhyolitic glass, is described together with salt beds in Pleistocene lacustrine sediments in Clayton valley, Nevada (Araoka et al., 2014; Munk et al., 2011), in several other locations in the North American Basin and Range Province (Vine and Dooley, 1980) and in Turkish boron-rich salt flats (Büyüburç and Köksal, 2005). Additionally, the existence of Li-bearing clays is hypothesized to explain the concentration and isotopic values of Li in deep strata in the Salar de Olaroz, Argentina (Garcia et al., 2020). No hectorite has been described in the SdA, although Ide and Kunasz (1990) emphasized the existence of Li concentrations as high as 484 ppm in the argillaceous sediments underlying the tuffs of the Miocene El Campamento Fm., present in the Cordillera de la Sal and the Cordón de Lila areas. Up to 200 mg/L of exchangeable Li was removed from synthetic Li-bearing smectites with 1 M NH_4Cl and Ca_2Cl solution prior to Li isotope fractionation experiments (Vigier et al., 2008), and higher concentrations are expected to be extracted with a halite-saturated brine (approximately 6 M NaCl).

To verify the feasibility of the above described hypothesis, only extensive water table data on the Li-Mg-rich brine is available (Marazuela et al., 2019a, 2019b), whereas chemical and isotopic data are scarce. These data are commonly property of mining companies, and if published, they have no spatial references (e.g., Munk et al., 2018). The enrichment of Li and other salts by dilute recharge is compatible with the atmospheric signature of the $^3He/^4He$ gas ratio and with the decrease in Na content as the Li content increases in the Li-rich brines reported by Munk et al. (2018). Additionally, the lack of a clear correlation between Li and Cl ($R^2 = 0.57$) reported by Hydrotechnica (1988) is less consistent with evaporative concentration. Unfortunately, the high correlations between Li and Mg ($R^2 = 0.98$) and

Li and K ($R^2 = 0.91$) in the data reported by Hydrotechnica (1988) and the heavier δ^7Li values of the Li-Mg-rich brines reported by Munk et al. (2018) are consistent with both evaporative concentration and dissolution of ancient salts and/or clay extraction.

Finally, it is important to highlight that the thermohaline convection of salt flats could not be easily identified in field observations. The shallowest aquifer of the nucleus does not show an appreciable increase in the water table associated with the SFS (Fig. 2). Because of this fact, the Ca-Cl-rich brine coming from the west-southwest can, after recirculation, overcome the SFS on its path to the minimum hydraulic head. Moreover, the most frequent physical-chemical parameters (density, electrical conductivity, total dissolved solids, etc.) do not give too much information about this fact, and detailed hydrochemical and isotopic analyses are necessary.

In future studies, the δ^2H and δ^{18}O isotopes of the Li-rich brine should readily reveal if the Li-Mg-rich brine comes from a highly evaporated brine or from dilute recharge water acquiring its salinity by dissolution of salt rocks and/or clay extraction. Additionally, an indirect test for dissolution of Li-rich salts or leaching of Li-rich clays could be the Br concentration of the Li-rich brines. Thus, due to the increasing concentration of the solution with evaporation and the higher solid/liquid partition coefficient of Mg salts (Marion et al., 2010), Br is expected to be enriched in the advanced evaporation salts hypothetically accompanying the Li salts (see Krupp, 2005 for a Permian example). Therefore, Br is expected to be present in the analyses of Li-Mg-rich brines. In contrast, Br is poorly scavenged by halite, and brines formed by recharge water dissolving halite and extracting Li from clays are not expected to have Br concentrations that differ greatly from those of the dilute inflows. Similarly, light δ^{11}B values would be more compatible with exchange with clays rather than dissolution of soluble salts or an advanced stage of evaporation, which would be expected to be associated with heavier isotopic values (Godfrey and Álvarez-Amado, 2020). Also, an accurate structural characterization of the SFS and its hydraulic parameters will help future numerical models to define faithfully local convection cells in the SFS.

5. Conclusions

Thermohaline flow modelling has demonstrated the critical effect of the minimum hydraulic head of the regional water table on the groundwater flow of salt flats. The minimum hydraulic head divides the basin into two isolated hydrodynamic systems and constitutes the endpoint towards which all flow paths converge and terminate, thereby representing the expected location of the most evaporated brines. The results show that the relatively cooler crust below de nucleus of the Salar de Atacama than below the volcanic arc is not an inconvenient for the developing of convection and upward flow along the Salar Fault System.

Thermohaline flow modelling has been useful in discussing the origin of the extreme Li enrichment in the Salar de Atacama. Firstly, a clear spatial mismatch between the locations of the Li-Mg-rich brines in the central-western zone of the nucleus (in the Salar Fault System) and the computed minimum hydraulic head of the water table in the easternmost zone of the nucleus has been stablished. Whatever the origin of the recharge solutes (weathering, leakage of present-day salt flats, leaching of buried salt flats or magmatic contribution, in the eastern flank of the SdA basin or in the Altiplano-Puna), this mismatch discards recent evaporative concentration of the recharge water as the current mechanism for reaching the extreme Li concentrations of the brines. On the contrary, only if the evaporation was more homogenous than the current one, would the minimum hydraulic head be located in the central-western zone of the nucleus. This hypothetical scenario could have occurred in previous stages of the Salar de Atacama formation and recorded in layers buried today below the current salt flat. Secondly, the persistence of a saline interface at depth, regardless of the temperature gradient, also precludes deep hydrothermal inflows heated below the volcanic arc to be the source of the Li-Mg-rich brines ascending along the Salar Fault System.

The results of the thermohaline flow modelling are compatible with the remobilization of ancient layers of Li-Mg-enriched salts and/or clays by dilute recharge waters coming from the western flank of the basin. The water recharged on the western flank of the basin quickly increases in density by dissolution of salts in the Cordillera de la Sal. Once incorporated to the nucleus, along its path towards the minimum hydraulic head, the brine can be captured by the convective circulation developed in the Salar Fault System. This enables its Li-Mg enrichment if a layer of ancient salt or clay enriched in these elements exists in depth. Here, the role of faults and density-driven flow is capital to allow efficient downward and upward flow rates that favour the remobilization of Li and Mg. Further chemical and isotopic analyses (major solutes, Br, δ^2H-δ^{18}O, δ^{11}B, etc.) of the Li-Mg-rich brines (to add to the scarce published information) are needed to confirm or discard the proposed hypothesis about the groundwater origin and the mechanism of Li enrichment in the Salar de Atacama.

CRediT authorship contribution statement

M.A. Marazuela: Conceptualization, Methodology, Investigation, Writing - original draft, Visualization, Software. **C. Ayora:** Conceptualization, Methodology, Investigation, Writing - review & editing, Supervision, Visualization. **E. Vázquez-Suñé:** Writing - review & editing. **S. Olivella:** Methodology, Writing - review & editing, Software. **A. García-Gil:** Methodology, Writing - review & editing, Software.

Declaration of competing interest

The authors declare that they have no known competing financial interests or personal relationships that could have appeared to influence the work reported in this paper.

Acknowledgements

The authors acknowledge Fabien Magri for sharing the *BrineDensity* plug-in and FEFLOW for sponsoring the license. The authors thank Craig Simmons and James Wards for sharing their experience during the modelling work and Juan Hidalgo for his fruitful contribution to the discussion. Finally, David Dempsey and an anonymous reviewer are greatly acknowledged for their comments and corrections which significantly improved the original version.

References

Alonso, H., Risacher, F., 1996. Geoquímica del Salar de Atacama, parte 1: Origen De Los componentes y balance salino. Rev. Geol. Chile 23, 113–122. https://doi.org/10.5027/andgeoV23n2-a01.

Alpers, C.N., Whittemore, D.O., 1990. Hydrogeochemistry and stable isotopes of ground and surface waters from two adjacent closed basins, Atacama Desert, northern Chile. Appl. Geochem. 5, 719–734. https://doi.org/10.1016/0883-2927(90)90067-F.

Araoka, D., Kawahata, H., Takagi, T., Watanabe, Y., Nishimura, K., Nishio, Y., 2014. Lithium and strontium isotopic systematics in playas in Nevada, USA: constraints on the origin of lithium. Miner. Depos. 49, 371–379. https://doi.org/10.1007/s00126-013-0495-y.

Arriagada, C., Cobbold, P.R., Roperch, P., 2006. Salar de Atacama basin: a record of compressional tectonics in the central Andes since the mid-Cretaceous. Tectonics 25, TC1008. https://doi.org/10.1029/2004TC001770.

Barcelona, H., Lelli, M., Norelli, F., Peri, G., Winocur, D., 2019. Hydrochemical and geological model of the Bañitos-Gollete geothermal system in Valle del Cura, main Andes Cordillera of San Juan, Argentina. J. S. Am. Earth Sci. 96, 102378. https://doi.org/10.1016/j.jsames.2019.102378.

Baspineiro, C.F., Franco, J., Flexer, V., 2020. Potential water recovery during lithium mining from high salinity brines. Sci. Total Environ. 720, 137523. https://doi.org/10.1016/j.scitotenv.2020.137523.

Benson, T.R., Coble, M.A., Rytuba, J.J., Mahood, G.A., 2017. Lithium enrichment in intracontinental rhyolite magmas leads to Li deposits in caldera basins. Nat. Commun. 8, 1–9. https://doi.org/10.1038/s41467-017-00234-y.

Blessent, D., Jørgensen, P.R., Therrien, R., 2014. Comparing discrete fracture and continuum models to predict contaminant transport in fractured porous media. Groundwater 52, 84–95. https://doi.org/10.1111/gwat.12032.

Bobst, A.L., Lowenstein, T.K., Jordan, T.E., Godfrey, L.V., Ku, T.L., Luo, S., 2001. A 106 ka paleoclimate record from drill core of the Salar de Atacama, northern Chile. Palaeogeogr. Palaeoclimatol. Palaeoecol. 173, 21–42. https://doi.org/10.1016/S0031-0182(01)00308-X.

Büyüburç, A., Köksal, G., 2005. An attempt to minimize the cost of extracting lithium from boron clays through robust process design. Clay Clay Miner. 53, 301–309. https://doi.org/10.1346/CCMN.2005.0530310.

Corenthal, L.G., Boutt, D.F., Hynek, S.A., Munk, L.A., 2016. Regional groundwater flow and accumulation of a massive evaporite deposit at the margin of the Chilean Altiplano. Geophys. Res. Lett. 43, 8017–8025. https://doi.org/10.1002/2016GL070076.

De Silva, S.L., 1989. Geochronology and stratigraphy of the ignimbrites from the 21° 30′ S to 23° 30′ S portion of the Central Andes of northern Chile. J. Volcanol. Geotherm. Res. 37, 93–131. https://doi.org/10.1016/0377-0273(89)90065-6.

Diersch, H.-J.G., 2014. FEFLOW: Finite Element Modeling of Flow, Mass and Heat Transport in Porous and Fractured Media. Springer-Verlag, Berlin Heidelberg https://doi.org/10.1007/978-3-642-38739-5.

Driesner, T., Heinrich, C.A., 2007. The system H2O-NaCl. Part I: correlation formulae for phase relations in temperature-pressure-composition space from 0 to 1000 °C, 0 to 5000 bar, and 0 to 1 XNaCl. Geochim. Cosmochim. Acta 71, 4880–4901. https://doi.org/10.1016/j.gca.2006.01.033.

Duffy, C.J., Al-Hassan, S., 1988. Groundwater circulation in a closed desert basin: topographic scaling and climatic forcing. Water Resour. Res. 24, 1675–1688. https://doi.org/10.1029/WR024i010p01675.

Eccles, D.R., Berhane, H., 2011. Geological Introduction to Lithium-Rich Formation Water with Emphasis on the Fox Creek Area of West-Central Alberta, Report 2011-10.

Eppelbaum, L., Kutasov, I., Arkady, P., 2014. Applied Geothermics. Springer-Verlag, Berlin Heidelberg https://doi.org/10.1007/978-3-642-34023-9.

Ericksen, G.E., Vine, J.D., Ballón, R., 1978. Chemical composition and distribution of lithium-rich brines in Salar de Uyuni and nearby salars in southwestern Bolivia. Energy 3, 355–363. https://doi.org/10.1016/0360-5442(78)90032-4.

Eugster, H.P., 1980. Geochemistry of evaporitic lacustrine deposits. Annu. Rev. Earth Planet. Sci. 8, 35–63.

Fan, Y., Duffy, C.J., Oliver, D.S., 1997. Density-driven groundwater flow in closed desert basins: field investigations and numerical experiments. J. Hydrol. 196, 139–184. https://doi.org/10.1016/S0022-1694(96)03292-1.

Garcia, M.G., Borda, L.G., Godfrey, L.V., López Steinmetz, R.L., Losada-Calderon, A., 2020. Characterization of lithium cycling in the Salar De Olaroz, Central Andes, using a geochemical and isotopic approach. Chem. Geol. 531, 119340. https://doi.org/10.1016/j.chemgeo.2019.119340.

Gardeweg, M., Ramírez, C.F., 1987. La Pacana caldera and the Atana ignimbrite. A major ash-flow and resurgent caldera complex in the Andes of northern Chile. Bull. Volcanol. 49, 547–566. https://doi.org/10.1007/BF01080449.

Garrett, D.E., 2004. Handbook of Lithium and Natural Calcium Chloride. Academic Press https://doi.org/10.1016/B978-0-12-276152-2.X5035-X.

Godfrey, L., Álvarez-Amado, F., 2020. Volcanic and saline lithium inputs to the Salar de Atacama. Minerals 10, 201. https://doi.org/10.3390/min10020201.

Godfrey, L.V., Chan, L.H., Alonso, R.N., Lowenstein, T.K., McDonough, W.F., Houston, J., Li, J., Bobst, A., Jordan, T.E., 2013. The role of climate in the accumulation of lithium-rich brine in the Central Andes. Appl. Geochem. 38, 92–102. https://doi.org/10.1016/j.apgeochem.2013.09.002.

Godfrey, L.V., Herrera, C., Gamboa, C., Mathur, R., 2019. Chemical and isotopic evolution of groundwater through the active Andean arc of Northern Chile. Chem. Geol. 518, 32–44. https://doi.org/10.1016/j.chemgeo.2019.04.011.

González, G., Cembrano, J., Aron, F., Veloso, E.E., Shyu, J.B.H., 2009. Coeval compressional deformation and volcanism in the central Andes, case studies from northern Chile (23°S–24°S). Tectonics 28, 1–18. https://doi.org/10.1029/2009TC002538.

Graf, T., Therrien, R., 2007. Coupled thermohaline groundwater flow and single-species reactive solute transport in fractured porous media. Adv. Water Resour. 30, 742–771. https://doi.org/10.1016/j.advwatres.2006.07.001.

Hamann, E., Post, V., Kohfahl, C., Prommer, H., Simmons, C.T., 2015. Numerical investigation of coupled density-driven flow and hydrogeochemical processes below playas. Water Resour. Res. 51, 9338–9352. https://doi.org/10.1002/2015WR017833.

Hamza, V.M., Dias, F.J.S.S., Gomes, A.J.L., Terceros, Z.G.D., 2005. Numerical and functional representations of regional heat flow in South America. Phys. Earth Planet. Inter. 152, 223–256. https://doi.org/10.1016/j.pepi.2005.04.009.

Hardie, L.A., 1990. The roles of rifting and hydrothermal CaCl2 brines in the origin of potash evaporites: an hypothesis. Am. J. Sci. 290, 43–106. https://doi.org/10.2475/ajs.290.1.43.

Hardie, L.A., 1991. On the significance of evaporites. Annu. Rev. Earth Planet. Sci. 19, 131–168. https://doi.org/10.1146/annurev.ea.19.050191.001023.

Hardie, L.A., Smoot, J.P., Eugster, H.P., 1978. Saline lakes and their deposits: A sediment approach. In: Matter, A., Tucker, M.E. (Eds.), Modern and Ancient Lake Sediments. International Association of Sedimentologists. Wiley-Blackwell, pp. 7–42. https://doi.org/10.1002/9781444303698.ch2.

Hirthe, E.M., Graf, T., 2015. Fracture network optimization for simulating 2D variable-density flow and transport. Adv. Water Resour. 83, 364–375. https://doi.org/10.1016/j.advwatres.2015.07.001.

Hofstra, A.H., Todorov, T.I., Mercer, C.N., Adams, D.T., Marsh, E.E., 2013. Silicate melt inclusion evidence for extreme pre-eruptive enrichment and post-eruptive depletion of lithium in silicic volcanic rocks of the Western United States: implications for the origin of Lithium-Rich Brines. Econ. Geol. 108, 1691–1701. https://doi.org/10.2113/econgeo.108.7.1691.

Holzbecher, E., 2005. Groundwater flow pattern in the vicinity of a salt lake. Hydrobiologia 532, 233–242.

Houston, J., 2006. Variability of precipitation in the Atacama Desert: its causes and hydrological impact. Int. J. Climatol. 26, 2181–2198. https://doi.org/10.1002/joc.1359.

Hydrotechnica, 1988. Salar de Atacama, Phase 3B, Hydrological Investigations. Santiago, Chile.

Ide, F., Kunasz, I.A., 1990. Origin of lithium in Salar de Atacama, Northern Chile. In: Ericksen, G.E., Cañas-Pinochet, M.T., Reinemund, J.A. (Eds.), Geology of the Andes and its Relation to Hydrocarbon and Mineral Resources. Houston, Texas, p. 452.

Irvine, D.J., Sheldon, H.A., Simmons, C.T., Werner, A.D., Griffiths, C.M., 2014. Investigation de l'influence de l'hétérogénéité d'un aquifère sur le potentiel de convection libre thermique dans l'aquifère du Yarragadee en Australie occidentale. Hydrogeol. J. 23, 161–173. https://doi.org/10.1007/s10040-014-1194-1.

Jayne, R.S., Pollyea, R.M., Dodd, J.P., Olson, E.J., Swanson, S.K., 2016. Spatial and temporal constraints on regional-scale groundwater flow in the Pampa del Tamarugal Basin, Atacama Desert, Chile. Hydrogeol. J. 24, 1921–1937. https://doi.org/10.1007/s10040-016-1454-3.

Jordan, T.E., Munoz, N., Hein, M., Lowenstein, T., Godfrey, L., Yu, J., 2002. Active faulting and folding without topographic expression in an evaporite basin, Chile. Bull. Geol. Soc. Am. 114, 1406–1421. https://doi.org/10.1130/0016-7606(2002)114<1406:AFAFWT>2.0.CO;2.

Jordan, T.E., Mpodozis, C., Muñoz, N., Blanco, N., Pananont, P., Gardeweg, M., 2007. Cenozoic subsurface stratigraphy and structure of the Salar de Atacama Basin, northern Chile. J. S. Am. Earth Sci. 23, 122–146. https://doi.org/10.1016/j.jsames.2006.09.024.

Karmanocky, F.J., Benison, K.C., 2016. A fluid inclusion record of magmatic/hydrothermal pulses in acid Salar Ignorado gypsum, northern Chile. Geofluids 16, 490–506. https://doi.org/10.1111/gfl.12171.

Kesler, S.E., Gruber, P.W., Medina, P.A., Keoleian, G.A., Everson, M.P., Wallington, T.J., 2012. Global lithium resources: relative importance of pegmatite, brine and other deposits. Ore Geol. Rev. 48, 55–69. https://doi.org/10.1016/j.oregeorev.2012.05.006.

Klyukin, Y.I., Driesner, T., Steele-MacInnis, M., Lowell, R.P., Bodnar, R.J., 2016. Effect of salinity on mass and energy transport by hydrothermal fluids based on the physical and thermodynamic properties of H2O-NaCl. Geofluids 16, 585–603. https://doi.org/10.1111/gfl.12181.

Kohfahl, C., Post, V.E.A., Hamann, E., Prommer, H., Simmons, C.T., 2015. Validity and slopes of the linear equation of state for natural brines in salt lake systems. J. Hydrol. 523, 190–195. https://doi.org/10.1016/j.jhydrol.2015.01.054.

Koltzer, N., Möller, P., Inbar, N., Siebert, C., Rosenthal, E., Magri, F., 2017. Thermal impacts of magmatic intrusions: a hypothesis of paleo-heating processes in the Tiberias Basin, Jordan-Dead Sea Transform. Energy Procedia 125, 80–87. https://doi.org/10.1016/j.egypro.2017.08.071.

Krupp, R.E., 2005. Formation and chemical evolution of magnesium chloride brines by evaporite dissolution processes - implications for evaporite geochemistry. Geochim. Cosmochim. Acta 69, 4283–4299. https://doi.org/10.1016/j.gca.2004.11.018.

Lever, D.A., Jackson, C.P., 1985. On the Equations for the Flow of Concentrated Salt Solution through a Porous Medium. Report No. DOE/RW85.100.

Li, Z., Chi, G., Bethune, K.M., 2016. The effects of basement faults on thermal convection and implications for the formation of unconformity-related uranium deposits in the Athabasca Basin, Canada. Geofluids 16, 729–751. https://doi.org/10.1111/gfl.12180.

Li, R., Liu, C., Jiao, P., Wang, J., 2018. The tempo-spatial characteristics and forming mechanism of Lithium-rich brines in China. China Geol 1, 72–83. https://doi.org/10.31035/cg2018009.

Lindsay, J.M., 2001. Magmatic evolution of the La Pacana caldera system, Central Andes, Chile: compositional variation of two cogenetic, large-volume felsic ignimbrites. J. Petrol. 42, 459–486. https://doi.org/10.1093/petrology/42.3.459.

Liu, W., Agusdinata, D.B., 2020. Interdependencies of lithium mining and communities sustainability in Salar de Atacama, Chile. J. Clean. Prod. 260, 120838. https://doi.org/10.1016/j.jclepro.2020.120838.

Liu, W., Agusdinata, D.B., Myint, S.W., 2019. Spatiotemporal patterns of lithium mining and environmental degradation in the Atacama Salt Flat, Chile. Int. J. Appl. Earth Obs. Geoinf. 80, 145–156. https://doi.org/10.1016/j.jag.2019.04.016.

López Steinmetz, R.L., Salvi, S., García, M.G., Peralta Arnold, Y., Béziat, D., Franco, G., Constantini, O., Córdoba, F.E., Caffe, P.J., 2018. Northern Puna Plateau-scale survey of Li brine-type deposits in the Andes of NW Argentina. J. Geochemical Explor. 190, 26–38. https://doi.org/10.1016/j.gexplo.2018.02.013.

Lowenstein, T.K., Risacher, F., 2009. Closed basin brine evolution and the influence of Ca-Cl inflow waters: death valley and Bristol dry Lake California, Qaidam Basin, China, and Salar de Atacama, Chile. Aquat. Geochemistry 15, 71–94. https://doi.org/10.1007/s10498-008-9046-z.

Lowenstein, T.K., Dolginko, L.A.C., García-Veigas, J., 2016. Influence of magmatic-hydrothermal activity on brine evolution in closed basins: Searles Lake, California. Bull. Geol. Soc. Am. 128, 1555–1568. https://doi.org/10.1130/B31398.1.

Magaritz, M., Aravena, R., Peña, H., Suzuki, O., Grilli, A., 1990. Source of ground water in the deserts of northern Chile: evidence of deep circulation of ground water from the Andes. Ground Water 28, 513–517.

Magri, F., 2009. Derivation of the coefficients of thermal expansion and compressibility for use in FEFLOW. FEFLOW White Papers. vol III, pp. 13–23.

Magri, F., Bayer, U., Maiwald, U., Otto, R., Thomsen, C., 2009. Impact of transition zones, variable fluid viscosity and anthropogenic activities on coupled fluid-transport processes in a shallow salt-dome environment. Geofluids 9, 182–194. https://doi.org/10.1111/j.1468-8123.2009.00242.x.

Magri, F., Akar, T., Gemici, U., Pekdeger, A., 2010. Deep geothermal groundwater flow in the Seferihisar-Balçova area, Turkey: results from transient numerical simulations of coupled fluid flow and heat transport processes. Geofluids 10, 388–405. https://doi.org/10.1111/j.1468-8123.2009.00267.x.

Magri, F., Akar, T., Gemici, U., Pekdeger, A., 2012. Numerical investigations of fault-induced seawater circulation in the Seferihisar-Balçova Geothermal system, western Turkey. Hydrogeol. J. 20, 103–118. https://doi.org/10.1007/s10040-011-0797-z.

Magri, F., Inbar, N., Siebert, C., Rosenthal, E., Guttman, J., Möller, P., 2015. Transient simulations of large-scale hydrogeological processes causing temperature and salinity anomalies in the Tiberias Basin. J. Hydrol. 520, 342–355. https://doi.org/10.1016/j.jhydrol.2014.11.055.

Magri, F., Möller, S., Inbar, N., Möller, P., Raggad, M., Rödiger, T., Rosenthal, E., Siebert, C., 2016. 2D and 3D coexisting modes of thermal convection in fractured hydrothermal systems - implications for transboundary flow in the Lower Yarmouk Gorge. Mar. Pet. Geol. 78, 750–758. https://doi.org/10.1016/j.marpetgeo.2016.10.002.

Marazuela, M.A., Vázquez-Suñé, E., Ayora, C., García-Gil, A., Palma, T., 2019a. Hydrodynamics of salt flat basins: the Salar de Atacama example. Sci. Total Environ. 651, 668–683. https://doi.org/10.1016/j.scitotenv.2018.09.190.

Marazuela, M.A., Vázquez-Suñé, E., Ayora, C., García-Gil, A., Palma, T., 2019b. The effect of brine pumping on the natural hydrodynamics of the Salar de Atacama: the damping capacity of salt flats. Sci. Total Environ. 654, 1118–1131. https://doi.org/10.1016/j.scitotenv.2018.11.196.

Marazuela, M.A., Vázquez-Suñé, E., Custodio, E., Palma, T., García-Gil, A., Ayora, C., 2018. 3D mapping, hydrodynamics and modelling of the freshwater-brine mixing zone in salt flats similar to the Salar de Atacama (Chile). J. Hydrol. 561, 223–235. https://doi.org/10.1016/j.jhydrol.2018.04.010.

Marazuela, M.A., Vázquez-Suñé, E., Ayora, C., García-Gil, A., 2020. Towards more sustainable brine extraction in salt flats: learning from the Salar de Atacama. Sci. Total Environ. 703, 135605. https://doi.org/10.1016/j.scitotenv.2019.135605.

Marion, G.M., Catling, D.C., Zahnle, K.J., Claire, M.W., 2010. Modeling aqueous perchlorate chemistries with applications to Mars. Icarus 207, 675–685. https://doi.org/10.1016/j.icarus.2009.12.003.

Mercer, J.W., Pinder, G.F., 1974. Finite element analysis of hydro-thermal systems. In: Oden, J.T., Zienkiewicz, O.C., Gallagher, R.H., Taylor, C. (Eds.), Finite Element Analysis of Hydro-Thermal Systems. University of Alabama Press, pp. 401–414.

Munk, L.A., Jochens, H., Jennings, M., Bradley, D.C., Hynek, S.A., Godfrey, L., 2011. Origin and evolution of Li-rich brines at Clayton Valley, Nevada, USA. 11th SGA Biennial Meeting. Antofagasta, Chile, pp. 217–219.

Munk, L.A., Hynek, S.A., Bradley, D., Boutt, D.F., Labay, K., Jochens, H., 2016. Lithium brines: a global perspective. Rev. Econ. Geol. 18, 339–365.

Munk, L.A., Boutt, D.F., Hynek, S.A., Moran, B.J., 2018. Hydrogeochemical fluxes and processes contributing to the formation of lithium-enriched brines in a hyper-arid continental basin. Chem. Geol. 493, 37–57. https://doi.org/10.1016/j.chemgeo.2018.05.013.

Muñoz, N., Charrier, R., Jordan, T., 2002. Interactions between basement and cover during the evolution of the Salar de Atacama Basin, northern Chile. Rev. Geológica Chile 29, 3–29. https://doi.org/10.4067/S0716-02082002000100004.

Nield, D.A., Simmons, C.T., Kuznetsov, A.V., Ward, J.D., 2008. On the evolution of salt lakes: episodic convection beneath an evaporating salt lake. Water Resour. Res. 44, W02439. https://doi.org/10.1029/2007WR006161.

Pananont, P., Mpodozis, C., Blanco, N., Jordan, T.E., Brown, L.D., 2004. Cenozoic evolution of the northwestern Salar de Atacama Basin, northern Chile. Tectonics 23, 1–19. https://doi.org/10.1029/2003TC001595.

Pueyo, J.J., Chong, G., Ayora, C., 2017. Lithium saltworks of the Salar de Atacama: a model for MgSO4-free ancient potash deposits. Chem. Geol. 466, 173–186. https://doi.org/10.1016/j.chemgeo.2017.06.005.

Reutter, K.J., Charrier, R., Gotze, H.J., Schurr, B., Wigger, P., Scheuber, E., Giese, P., Reuther, C.D., Schmidt, S., Rietbrock, A., Chong, G., Belmonte-Pool, A., 2006. The Salar de Atacama Basin: A Subsiding Block within the Western Edge of the Altiplano-Puna Plateau. Andes Act. Subduction Orogeny. , pp. 303–325. https://doi.org/10.1007/978-3-540-48684-8_14.

Risacher, F., Alonso, H., 1996. Geoquímica del Salar de Atacama, parte 2: Evolución de las aguas. Rev. Geol. Chile 23, 123–134.

Risacher, F., Fritz, B., 1991. Geochemistry of Bolivian salars, Lipez, southern Altiplano: origin of solutes and brine evolution. Geochim. Cosmochim. Acta 55, 687–705. https://doi.org/10.1016/0016-7037(91)90334-2.

Risacher, F., Fritz, B., 2009. Origin of salts and brine evolution of Bolivian and Chilean salars. Aquat. Geochemistry 15, 123–157. https://doi.org/10.1007/s10498-008-9056-x.

Risacher, F., Alonso, H., Salazar, C., 2003. The origin of brines and salts in Chilean salars: a hydrochemical review. Earth-Science Rev 63, 249–293. https://doi.org/10.1016/S0012-8252(03)00037-0.

Rissmann, C., Leybourne, M., Benn, C., Christenson, B., 2015. The origin of solutes within the groundwaters of a high Andean aquifer. Chem. Geol. 396, 164–181. https://doi.org/10.1016/j.chemgeo.2014.11.029.

Rosen, M.R., 1994. The importance of groundwater in playas: a review of playa classifications and the sedimentology and hydrology of playas. Geol. Soc. Am. Spec. Pap. 289, 1–18. https://doi.org/10.1130/SPE289-p1.

Sanford, W.E., Wood, W.W., 1991. Brine evolution and mineral deposition in hydrologically open evaporite basins. Am. J. Sci. https://doi.org/10.2475/ajs.291.7.687.

Schmitt, A.K., 2001. Gas-saturated crystallization and degassing in large-volume, crystal-rich dacitic magmas from the Altiplano-Puna, northern Chile. J. Geophys. Res. Solid Earth 106, 30561–30578. https://doi.org/10.1029/2000jb000089.

Schoofs, S., Hansen, U., 2000. Depletion of a brine layer at the base of ridge-crest hydrothermal systems. Earth Planet. Sci. Lett. 180, 341–353. https://doi.org/10.1016/S0012-821X(00)00184-9.

Schurr, B., Rietbrock, A., 2004. Deep seismic structure of the Atacama basin, northern Chile. Geophys. Res. Lett. 31, 10–13. https://doi.org/10.1029/2004GL019796.

Shafabakhsh, P., Fahs, M., Ataie-Ashtiani, B., Simmons, C.T., 2019. Unstable density-driven flow in fractured porous media: the fractured elder problem. Fluids 4, 168. https://doi.org/10.3390/fluids4030168.

Shao, Q., Fahs, M., Younes, A., Makradi, A., Mara, T., 2016. A new benchmark reference solution for double-diffusive convection in a heterogeneous porous medium. Numer. Heat Transf. Part B Fundam. 70, 373–392. https://doi.org/10.1080/10407790.2016.1215718.

Shewchuk, J.R., 1996. Triangle: Engineering a 2D quality mesh generator and delaunay triangulator. In: Lin, M.C., Manocha, D. (Eds.), Applied Computational Geometry Towards Geometric Engineering. WACG 1996. Lecture Notes in Computer Science. Springer, Berlin, Heidelberg, pp. 203–222. https://doi.org/10.1007/BFb0014497.

Simmons, C.T., Narayan, K.A., Wooding, R.A., 1999. On a test case for density-dependent groundwater flow and solute transport models: the salt lake problem. Water Resour. Res. 35, 3607–3620. https://doi.org/10.1029/1999WR900254.

Simms, M.A., Garven, G., 2004. Thermal convection in faulted extensional sedimentary basins: theoretical results from finite-element modeling. Geofluids 4, 109–130. https://doi.org/10.1111/j.1468-8115.2004.00069.x.

Song, W., Gang, H., Ma, Y., Yang, S., Mu, B., 2017. Migration behavior of lithium during brine evaporation and KCl production plants in Qarhan salt Lake. Minerals 7. https://doi.org/10.3390/min7040057.

Tejeda, I., Cienfuegos, R., Muñoz, J.F., Durán, M., 2003. Numerical modeling of saline intrusion in Salar de Atacama. J. Hydrol. Eng. 8, 25–34. https://doi.org/10.1061/(ASCE)1084-0699(2003)8:1(25).

USGS, 2019. Minneral commodities summary. [WWW Document]. URL. https://www.usgs.gov/centers/nmic/mineral-commodity-summaries.

Vásquez, C., Ortiz, C., Suárez, F., Muñoz, J.F., 2013. Modeling flow and reactive transport to explain mineral zoning in the Atacama salt flat aquifer, Chile. J. Hydrol. 490, 114–125. https://doi.org/10.1016/j.jhydrol.2013.03.028.

Vigier, N., Decarreau, A., Millot, R., Carignan, J., Petit, S., France-Lanord, C., 2008. Quantifying Li isotope fractionation during smectite formation and implications for the Li cycle. Geochim. Cosmochim. Acta 72, 780–792. https://doi.org/10.1016/j.gca.2007.11.011.

Vine, J.D., Dooley, J.R., 1980. Where on Earth Is all the Lithium? https://doi.org/10.3133/ofr801234

Vujević, K., Graf, T., Simmons, C.T., Werner, A.D., 2014. Impact of fracture network geometry on free convective flow patterns. Adv. Water Resour. 71, 65–80. https://doi.org/10.1016/j.advwatres.2014.06.001.

Warren, J.K., 2010. Evaporites through time: tectonic, climatic and eustatic controls in marine and nonmarine deposits. Earth-Science Rev 98, 217–268. https://doi.org/10.1016/j.earscirev.2009.11.004.

Warren, J.K., 2016. Evaporites. A geological compendium, Evaporites. Springer https://doi.org/10.1007/978-3-319-13512-0.

Wood, W.W., Sanford, W.E., 1990. Ground-water control of evaporite deposition. Econ. Geol. 85, 1226–1235. https://doi.org/10.2113/gsecongeo.85.6.1226.

Wooding, R.A., Tyler, S.W., White, I., 1997. Convection in groundwater below an evaporating salt Lake: 1. Onset of instability. Water Resour. Res. 33, 1199–1217. https://doi.org/10.1029/96WR03533.

Yechieli, Y., Wood, W.W., 2002. Hydrogeologic processes in saline systems: playas, sabkhas, and saline lakes. Earth-Science Rev 58, 343–365. https://doi.org/10.1016/S0012-8252(02)00067-3.

Yu, J.Q., Gao, C.L., Cheng, A.Y., Liu, Y., Zhang, L., He, X.H., 2013. Geomorphic, hydroclimatic and hydrothermal controls on the formation of lithium brine deposits in the Qaidam Basin, northern Tibetan Plateau, China. Ore Geol. Rev. 50, 171–183. https://doi.org/10.1016/j.oregeorev.2012.11.001.

Zatout, M., López Steinmetz, R.L., Hacini, M., Fong, S.B., M'nif, A., Hamzaoui, A.H., López Steinmetz, L.C., 2020. Saharan lithium: brine chemistry of chotts from eastern Algeria. Appl. Geochem. 115. https://doi.org/10.1016/j.apgeochem.2020.104566.

Zechner, E., Dresmann, H., Mocuţa, M., Danchiv, A., Huggenberger, P., Scheidler, S., Wiesmeier, S., Popa, I., Zlibut, A., 2019. Salt dissolution potential estimated from two-dimensional vertical thermohaline flow and transport modeling along a Transylvanian salt diapir, Romania. Hydrogeol. J. 27, 1245–1256. https://doi.org/10.1007/s10040-018-1912-1.